FACULTY OF SCIENCE
UNIVERSITY OF COPENHAGEN

Bachelor Thesis

by Karsten Bjerrum Dideriksen, TCS224

A Laser System for a Deterministic Single Photon Source

Supervisor: Prof. Eugene S. Polzik, QUANTOP, Niels Bohr Institute

June 11, 2014

Abstract

This bachelor thesis presents and investigates a laser system consisting of an extended cavity diode laser and triangular cavities intended as the light source for a single photon source. The requirements for the light source in the single photon source are explained, and a theoretical treatment of triangular cavities is carried out showing that the triangular cavity has frequency filtering properties that are sensitive to the polarization and horizontal symmetry of the cavity modes as oppose to the more common standing wave cavity.

To verify the cavity properties an evacuable cavity is studied experimentally with the laser locked to another cavity through optical feedback. The cavity bandwidth is determined in a cavity ring-down measurement to be 72 kHz, and a cavity spectrum shows the theoretically expected resonances with some modification including a phase shift for the low-finesse polarization.

The filtering capabilities of the cavity are estimated in a detailed calculation where imperfect mode match is taken into account by calculating the power distribution on the cavity modes through an overlap integral. The calculation shows a filter ratio less than $1{:}10^{-6}$ which encourages to continue working with this cavity design.

Contents

1 Introduction

Quantum information technologies receive a lot of attention presently, especially from the science community as a promising path to unbreakable communication encryption and new ways for automated computation, but also in the general public where one of the latest examples is the appointment of quantum teleportation as the Danish research breakthrough of the year 2013 by the Danish newspaper Ingeniøren [ing.dk].

Optical physics is known as a field where quantum effects are observable without excessive noise [Knill et al.]. Therefore it is a promising path to realizing functional quantum information technologies (e.g single photons, cavity quantum electrodynamics, trapped atomic ions) in competition with other fields such as quantum photonics (quantum dots) and condensed matter electronics (superconducting qubits, single-electron-based qubits) [Ladd et al.].

A particular goal for the quantum information technology is the quantum simulator [Lloyd], a device capable of simulating many-body quantum systems at a speed much higher than classical (super)computers. The concept requires the interaction of several quantum bits, and currently the challenge for the variety of proposed and demonstrated applications is *scalability* [Ladd et al.].

In atomic physics and the context of this work a common realization of a quantum bit is a single photon which has the strong advantage that quantum computation can be achieved through the means of linear optics (beam splitters, phase shifters and photo-detectors) [Knill et al.], a well-known and highly industrialized technology. Though a variety of single photon sources have been demonstrated, there continues to be a demand for high-efficiency sources (efficiency: ratio between the energies of the stored and retrieved pulses, [Lvovsky et al.]). Working with a single photon a way of thinking about the efficiency is as the average succes probability. Suppose a source has a 80% efficiency then the probability of emitting a single photon is 80% per attempt, and combining 100 sources will have the probability of a collective emission of $0.8^{100} = 2 \cdot 10^{-10}$. A source like that will not be sufficient as quantum simulator backbone.

A workaround the efficiency challenge is to introduce a quantum state memory in the single photon source such that the single photon can be generated and retrieved on demand. If combining several sources of this type, one will simply have to wait for all photons to be generated and then retrieve all at once.

1.1 The Deterministic Single Photon Source

A new design for an on-demand single photon source is currently being investigated at QUANTOP, Niels Bohr Institute. The design is based on room temperature vapor cells which have the advantage of easy scalability as no cooling is needed. A schematic drawing of the single photon source setup can be seen in Figure 1.

The vapor cell contains caesium atoms, ^{133}Cs, and has a special coating that will allow a decoherence time $T_2 \approx 5\,\text{ms}$ (for definition see [Ladd et al.]). The Cs-cell will act as an atomic quantum memory when a weak excitation beam (10^9 photons) creates a single collective excitation meaning a quantum state where a single atom is excited, and the atom ensemble is in a superposition of any atom being the excited:

$$|\psi\rangle \propto \sum_{j=1}^{N} c_j \, |g_1 g_2 \ldots s_j \ldots g_N\rangle \,, \tag{1}$$

where the g_i and s_i states refer to the hyperfine sublevels of the caesium atom, and g_i is the excited state of the D_2 line of atom i, see Figure 2. When the excitation is created a heralding single photon will be emitted into the same spatial mode as the excitation beam but with the opposite polarization. In order to detect the single photon it is required to filter out the excitation beam. This is done in two steps: 1) A polarizing beam splitter filters out most of the beam, but some will leak into 2) a narrowband filter cavity where the excitation beam will be reflected and the single photon transmitted due to their frequency difference of $\delta\nu_\text{w} \equiv 9.192\,631\,770\,\text{GHz}$ which is

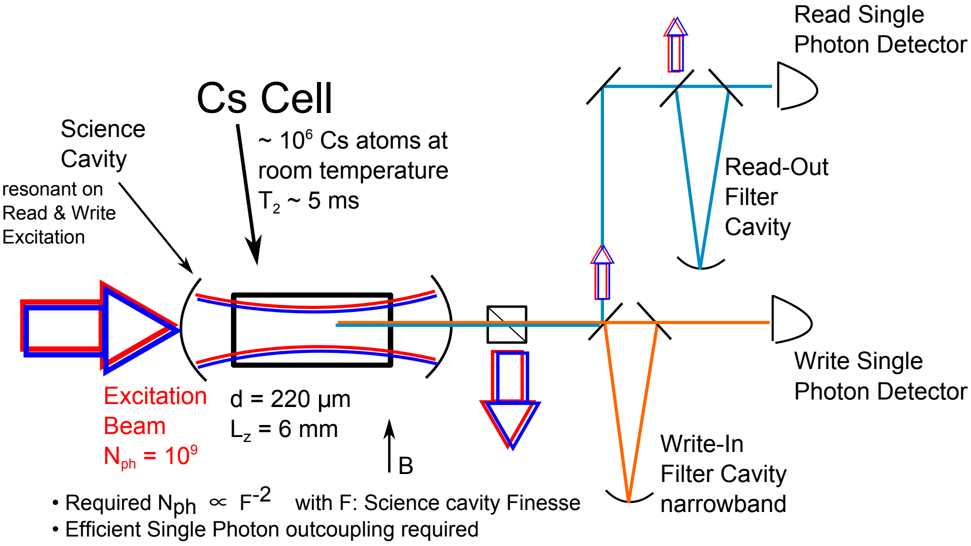

Figure 1: The single photon source setup. The Cs-cell inside the Science Cavity acts as a quantum memory. An excitation beam is applied to store a single photon in the cell. A successful write-in is heralded by a single photon which in order to be detected is filtered out from the excitation beam in two steps: 1) a polarizing beam splitter and 2) a filter cavity. Within the decoherence time $T_2 \approx 5\,\text{ms}$ the single photon can be retrieved by applying a new excitation beam.

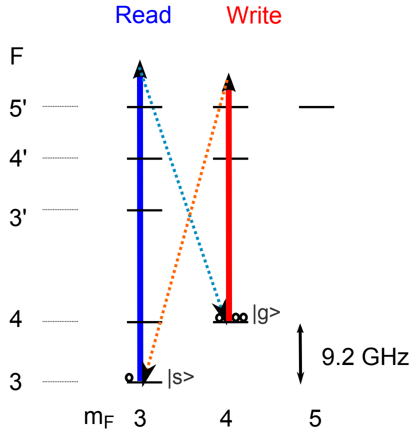

Figure 2: Atomic level scheme for the write and read processes. The cell contains caesium atoms in the state $|g\rangle$. Applying the write excitation beam (red line) detuned with respect to the D_2 line creates an atomic single collective excitation with one atom in the state $|s\rangle$, and in the process a heralding single photon is emitted (orange line).
Applying the read excitation beam (blue line), also detuned with respect to the D_2 line, return the atomic ensemble to all atoms in the $|g\rangle$ state by emitting the stored single photon (cyan line). The $|g\rangle\,, |s\rangle$ states refer to the hyperfine sublevels of the caesium atom.

the D_2 transition of the caesium atom that defines the second [BIPM]. Hereafter the heralding photon can be detected in a single photon detector.

Similarly the single photon can be retrieved by applying another weak laser beam which has to be filtered out afterwards in order to output only the single photon.

Simulations done at QUANTOP have shown that the optimal excitation probability per attempt to write is approximately 2%, and with the possibility of initializing a new attempt to write every 10 µs the average success time becomes $10\,\mu s/0.02 = 0.5\,ms$ which is way less than the decoherence time $T_2 \approx 5\,ms$. The simulations predict a retrieval efficiency of the write-in process of 55%.

As a benchmark other groups have reached fairly good storage times and retrieval efficiencies, examples are: >30% for a storage time of 22 µs using three-level atomic gradient echo memory [Higgimbottom et al.], a $1/e$ storage time of 1 ms using cold ^{87}Rb atomic ensemble in a magneto-optical trap at a temperature of about 100 µK [Zhao, Chen et al.], prolonged lifetime of up to 16 s in an ultracold atomic gas confined in a one-dimensional optical lattice [Dudin et al.] (however, this is measured from the pulse energy at 38 ms where efficiency is already 14%).

1.2 DLCZ Quantum Repeater Scheme

An example of where the single photon source could have its application is the DLCZ quantum repeater scheme named after the inventors L.-M. Duan, M.D. Lukin, J.I. Cirac, and P. Zoller. The idea of the scheme is to reduce the loss of quantum information with distance; for simple quantum information transmission this scales exponentially [DLCZ]. The scheme proposes to divide the transmission channel into several segments each comparable to the attenuation length. When entanglement is generated in all segments an attempt to entangle two adjacent segments can be made in order to extent the transmission channel. Some attempts will succeed and some will fail why it is important to incorporate a quantum memory to keep the succeeded entangled segments alive until all segment pairs are entangled. Then the process is repeated to entangle segment pairs until the full channel is established. The inventors have shown that in this scheme the loss of quantum information will scale only polynomially with distance [DLCZ]. The inventors proposed to use photonic quantum bits and atomic ensembles as quantum memory much similar to the design of the single photon source currently under construction.

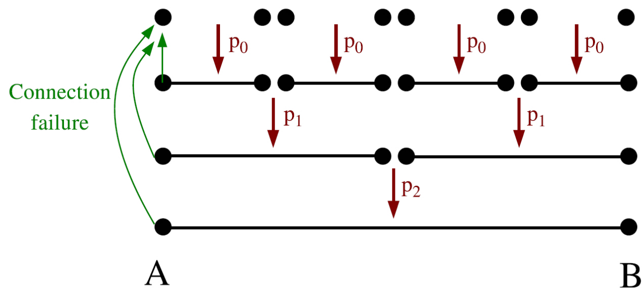

Figure 3: The basic idea of the DLCZ quantum repeater scheme. The communication channel from A to B is divided into several segments that individually can be established as channel via entanglement with a certain propability for success p_i. When each segment channel is established two adjacent segments can be entangled to extent the channel. If an attempt to establish entanglement fails, the process will start over in that segment while the rest wait and keep the channel open. Figure from [Petersen].

1.3 A Laser System for the Single Photon Source

At the current stage of the single photon source setup at QUANTOP two central features of the laser system which is intended for the excitation beam, are being investigated:

1) The linewidth of the laser system. The single photon has to be filtered using a narrowband cavity, and the excitation laser linewidth should not be broader than this. When the excitation beam is applied to retrieve the single photon the beam will determine the frequency of the single photon. If it is broader than the cavity bandwidth, it will not be transmitted properly. Simulations have shown that the necessary linewidth is 10 kHz. To obtain this the laser will be locked to a high-finesse cavity through optical feedback.

2) The filtering capability of the narrowband filter cavity. In order to ensure that the heralding single photon can be detected with a high degree of certainty, it is required to filter out the excitation beam. A Glan-Thompson polarizing beam splitter will transmit (leak) 10^{-5} of the reflection polarization [Thorlabs], and thus the filter cavity needs to filter out the leaked excitation beam with a ratio of $1{:}10^4$ to transmit less than one photon to the single photon detector.

The present bachelor project sets out to setup and investigate a suggested laser system for the single photon source with a special interest in the two mentioned features. Emphasis has been on delivering a permanent structure that is intended to function as the laser system for the single photon source. Therefore much attention has been paid to details and a thorough understanding of the system.

2 Theoretical Cavity Approach

In the experiment two triangular cavities are used to control laser output and filtering, respectively. Though the cavities have different geometries (see section 3) they behave very much alike and will in the following be treated as a general triangular cavity.

The idea of using mirrors to form an optical resonator (i.e. cavity) is widespread and have been thoroughly analysed [Kogelnik & Li]. However, the common use and treatment is of standing wave cavities where two mirrors are positioned in the optical path of the laser beam. As the following will show the triangular cavity requires a treatment of its own as it differs from the standing wave cavity on several features.

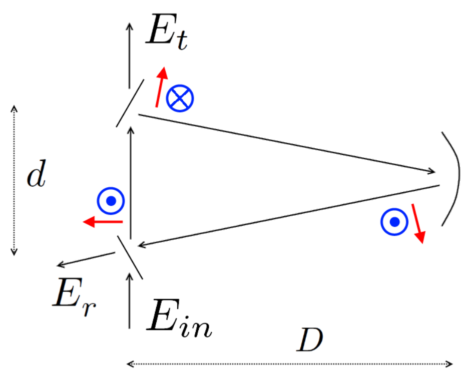

Figure 4: Sketch of the path of light through the triangular cavity. $E_{\rm in}, E_{\rm r}, E_{\rm t}$ are the electric fields of the incoming, reflected and transmitted light, respectively. Red arrows mark the axis of which the E-field of p-polarized light is measured along. In this definition *no* π phase shift is acquired upon reflection (cf. the Fresnel formulas, [Milonni & Eberly, p. 210]). Blue 'arrows' indicate that a π phase shift *is* acquired upon reflection for s-polarized light.

2.1 Cavity Transmission and Reflection

In this treatment it is sufficient to express the beam behaviour solely by its electric field component, and a plane wave description is adopted: $E(z) = \mathcal{E}(z)e^{i(kz-\omega t)}$. We consider a cavity consisting of three mirrors, two flat for in- and outcoupling and one curved, as indicated in Figure 4. Each mirror can be specified by a polarization dependent reflectivity, R_i, and transmission coefficient, $T_i \equiv 1 - R_i$, where the definitions refer to beam intensity. Therefore the reflected E-field becomes $E_\mathrm{r} = \sqrt{I_\mathrm{r}} = \sqrt{R_i I_\mathrm{in}} = \pm\sqrt{R_i}E_\mathrm{in}$ where the sign is polarization dependent and determined by the Fresnel formulas [Milonni & Eberly, p. 210]. For an s-polarized incoming beam, E^s_in, as indicated in Figure 4 the beam after one round trip can be expressed as

$$E^\mathrm{s}_\mathrm{RT}(0) = \sqrt{T_1 R_2 R_3} E^\mathrm{s}_\mathrm{in}(0) e^{ikL}, \tag{2}$$

where L is the round trip length. If assuming a continuous wave input (i.e. $\mathcal{E}$ time independent), the steady-state solution to the cavity field just after the incoupling mirror ($z = 0$) can be written as

$$E^\mathrm{s}_\mathrm{cav}(0) = -\sqrt{R_1 R_2 R_3} E^\mathrm{s}_\mathrm{cav}(0) e^{ikL} + \sqrt{T_1} E^s_\mathrm{in}(0) \tag{3}$$

$$\Leftrightarrow E^\mathrm{s}_\mathrm{cav}(0) = \frac{\sqrt{T_1}}{1 + \sqrt{R_1 R_2 R_3} e^{ikL}} E^\mathrm{s}_\mathrm{in}(0). \tag{4}$$

The minus in the first term in (3) comes from the beam picking up a π phase shift on every mirror reflection. This happens only for the s-polarization which is explained in Figure 4. From (4) the cavity reflection and transmission can be expressed

$$E^\mathrm{s}_\mathrm{r}(0) = -\sqrt{R_1} E^\mathrm{s}_\mathrm{in}(0) + \sqrt{T_1 R_2 R_3} E^\mathrm{s}_\mathrm{cav}(0) e^{ikL}, \tag{5}$$

$$\begin{aligned} E^\mathrm{s}_\mathrm{t}(d) &= \sqrt{T_2} E^\mathrm{s}_\mathrm{cav}(d) \\ &= \frac{\sqrt{T_1 T_2}}{1 + \sqrt{R_1 R_2 R_3} e^{ikL}} E^\mathrm{s}_\mathrm{in}(d), \end{aligned} \tag{6}$$

where d is the distance between the incoupling and the outcoupling mirror. Again the sign of the first term in (5) is polarization dependent. The cavity transmission dependency of mirror reflectivities and round trip length can be establish from (6)

$$\begin{aligned} T^\mathrm{s}_\mathrm{cav} &= \frac{I_\mathrm{t}}{I_\mathrm{in}} = \frac{|E^\mathrm{s}_\mathrm{t}(d)|^2}{|E^\mathrm{s}_\mathrm{in}(0)|^2} \\ &= \frac{T_1 T_2}{\left(1 - \sqrt{R_1 R_2 R_3}\right)^2 \left(1 + \frac{4\sqrt{R_1 R_2 R_3}}{\left(1-\sqrt{R_1 R_2 R_3}\right)^2} \cos^2 \frac{kL}{2}\right)} \\ &\equiv \frac{T_\mathrm{max}}{1 + F \cos^2 \frac{kL}{2}} \,. \end{aligned} \tag{7}$$

Evidently T_max is the intensity fraction transmitted on resonance

$$T_\mathrm{max} = \frac{T_1 T_2}{\left(1 - \sqrt{R_1 R_2 R_3}\right)^2} \,. \tag{8}$$

For a p-polarized incoming beam the cavity transmission, when changing the above mentioned signs, reads instead

$$T^\mathrm{p}_\mathrm{cav} = \frac{T_\mathrm{max}}{1 + F \sin^2 \frac{kL}{2}} \,. \tag{9}$$

The free spectral range (FSR) is defined as the distance between peaks of the same mode in the transmission spectrum $\Delta k_\mathrm{FSR} L = 2\pi$. (9) shows that the two polarizations are shifted by half the FSR. This is a unique feature of the triangular cavity in comparison with the standing wave equivalent and arises from the cavity having an odd number of mirrors.

It is possible to determine the bandwidth of the cavity defined as FWHM of the transmission by

$$\frac{1}{2} = \frac{1}{1 + F \sin^2 \frac{\delta k L}{4}} \tag{10}$$

$$\Leftrightarrow \delta k L = \frac{4}{\sqrt{F}} \,, \tag{11}$$

where the assumption of a very sharp peak (i.e. $\sqrt{F} >> 1$) allows only going to first order in δk. Expressing this as a frequency using $kc = 2\pi\nu$ yields

$$\delta\nu_{\mathrm{c}} = \frac{2c}{\pi L \sqrt{F}} \,. \tag{12}$$

The finesse of the cavity is defined as the ratio of the FSR to the half-width of the frequency band centered on a resonance frequency [Milonni & Eberly, p. 225]

$$\mathcal{F} = \frac{\Delta k_{\mathrm{FSR}}}{\delta k} = \frac{1}{2}\pi\sqrt{F} = \frac{\pi \sqrt[4]{R_1 R_2 R_3}}{1 - \sqrt{R_1 R_2 R_3}} \,. \tag{13}$$

Similar to the standing-wave cavity this is solely dependent on the mirror reflectivities or in other words the leakage from the cavity. Because the reflectivities of the mirrors are polarization dependent it is relevant to name the polarizations as respectively high- and low-finesse polarization.

The cavity bandwidth, $\delta\nu_{\mathrm{c}}$, is connected to the photon lifetime in the cavity. On a cavity round trip the light power changes as

$$\frac{-dP}{P} = (1 - R_1 R_2 R_3) = (1 + \sqrt{R_1 R_2 R_3})(1 - \sqrt{R_1 R_2 R_3}) = (1 + \sqrt{R_1 R_2 R_3})\frac{2\sqrt[4]{R_1 R_2 R_3}}{\sqrt{F}} \approx \frac{4}{\sqrt{F}} \,, \tag{14}$$

with the approximation $R_1, R_2, R_3 \approx 1$. Combining (14) with the round trip time $t_{\mathrm{c}} = L/c$ and (12) we get:

$$\frac{dP}{dt} = \frac{4c}{L\sqrt{F}} = 2\pi\delta\nu_{\mathrm{c}}. \tag{15}$$

Writing this on the exponential form we see the relation with the photon lifetime:

$$P = P_0 e^{-t/\tau_{\mathrm{c}}} = P_0 e^{-2\pi\delta\nu_{\mathrm{c}} t} \,, \tag{16}$$

where τ_{c} is the photon lifetime.

The above treatment does not consider internal cavity losses such as surface scattering due to non-ideal surfaces. Losses can, however, be included as a reduced reflectivity of the curved mirror as light transmitted through the mirror is just lost. The effect of losses is as expected a lower transmission, T_{max}, and finesse, $\mathcal{F}$, cf. (8) and (13).

Apart from having a significance for the cavity transmission the curved mirror also defines the transverse size of the resonant light modes. A laser resonator can be modelled as a series of lenses [Kogelnik & Li]. In the case of the triangular cavity where only one curved mirror is involved, it is a series of identical lenses with focal length half the length of the radius of curvature $f = R_{\mathrm{c}}/2$ separated by distance L. The resonant beam will fulfil the condition that the beam radius of curvature just changes sign going through each lens (i.e. $R_{\mathrm{c1}} = -R_{\mathrm{c2}}$). According to [Kogelnik & Li] the change in radius of curvature of the incoming beam can be expressed as

$$\frac{1}{R_{\mathrm{c2}}} = \frac{1}{R_{\mathrm{c1}}} - \frac{1}{f} \,. \tag{17}$$

The resonance condition is fulfilled when the mirror curvature equals the beam radius of curvature, $R_\mathrm{c} = R_\mathrm{c1}$. From here it is possible to calculate the cavity mode waist size w_0 [Kogelnik & Li]

$$R_\mathrm{c} = \frac{L}{2}\left[1 + \left(\frac{2\pi w_0^2}{\lambda L}\right)^2\right] \tag{18}$$

$$\Leftrightarrow w_0^2 = \frac{\lambda}{2\pi}\sqrt{L(2R_\mathrm{c} - L)}\,. \tag{19}$$

Note that the implied resonance condition holds only for a beam of normal incidence on the curved mirror. This is not the case with the triangular cavity. However, if the distance from the flat mirrors to the curved one is large compared to the distance between the flat mirrors (for our setup $d \approx 20\,\mathrm{mm}$ compared to the distance to the curved mirror, $D \approx 750\,\mathrm{mm}$), the incidence is approximately normal.

2.2 Transversal Mode Resonances

The model for cavity resonances can be expanded by including a more realistic laser beam description than a plane wave. The solutions to the scalar wave equation can be expressed in the complete basis of Hermite-Gaussian transversal modes [Kogelnik & Li]

$$E_{lm}(\mathbf{r}) = A_{lm} H_l\left(\frac{\sqrt{2}x}{w(z)}\right) H_m\left(\frac{\sqrt{2}y}{w(z)}\right) e^{-\frac{\rho^2}{w^2(z)} - i\phi_{lm}(z)}, \tag{20}$$

$$\phi_{lm}(\mathbf{r}) = kz + k\frac{\rho^2}{2R_\mathrm{c}(z)} - (l+m+1)\arctan\frac{z}{z_\mathrm{R}}\,, \tag{21}$$

where A_{lm} is the mode amplitude, H_l is the l'th order Hermite polynomial, $R_\mathrm{c}(z) = z\left[1 + (z_\mathrm{R}/z)^2\right]$ is the beam radius of curvature, $w(z) = w_0^2\left[1 + (z/z_\mathrm{R})^2\right]$ is the beam radius, $z_\mathrm{R} = \pi w_0^2/\lambda$ is the Rayleigh length, λ is wavelength, w_0 is the beam waist size and $\rho^2 = x^2 + y^2$.

From (21) it is clear that the phase evolution along z is different for different higher order transversal modes. This affects the resonance frequency of those modes. For the mode to be resonant it must pick up a multiple of 2π on a round trip in the cavity if the beam is p-polarized (cf. Figure 4). That means for p-polarized light:

$$\phi_{lm}\left(z = \frac{L}{2}\right) - \phi_{lm}\left(z = \frac{-L}{2}\right) = kL - (l+m+1)\left(\tan^{-1}\frac{L}{2z_\mathrm{R}} - \tan^{-1}\frac{-L}{2z_\mathrm{R}}\right) = 2n\pi, \tag{22}$$

with $n = 0, 1, 2, ...$ Here the R_c dependent term of (21) is excluded because it only determines waist size which is dealt with in previous subsection. (22) can be reduced by using the relations written below (21) [Milonni & Eberly, p. 296] to

$$2n\pi = kL - (l+m+1)\arccos\left(1 - \frac{L}{R_\mathrm{mirror}}\right) \equiv kL - (l+m+1)\alpha\,, \tag{23}$$

where R_mirror is the radius of curvature for the curved cavity mirror. However, there is a correction to (23). Because the triangular cavity has an odd number of mirrors one round trip will generate a mirror image of the initial image (i.e. flipping the horizontal axis). Choosing x as the axis in the plane of the cavity (in our case horizontal) it means that for odd l the resonance frequency is shifted by half an FSR. Including this feature the resonance condition becomes

$$2n\pi = \begin{cases} kL - (l+m+1)\alpha - \left(1 - (-1)^l\right)\frac{\pi}{2} & \text{p-polarized} \\ kL - (l+m+1)\alpha - \left(1 + (-1)^l\right)\frac{\pi}{2} & \text{s-polarized.} \end{cases} \tag{24}$$

Figure 5 is a drawing of the resonances of the filter cavity where the position of the frequency of the excitation pulse folded back on the free spectral range is marked.

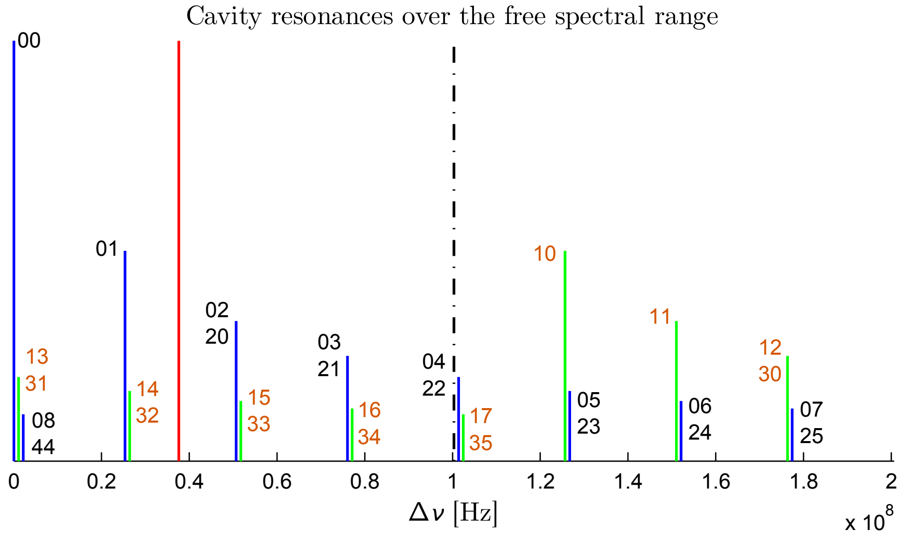

Figure 5: Cavity resonances over the free spectral range for the Evacuable Cavity. Blue lines mark the position of the first eight resonant frequencies for horizontally symmetric modes (i.e. even l) with mode numbering in black. Green lines mark the position of the first eight resonant frequencies for horizontally antisymmetric modes (odd l) with mode numbering in orange. Frequencies denote the resonance frequency difference from the 00-mode, $\Delta\nu$, of the single photon. The red line marks the frequency of the excitation pulse $\delta\nu_{\mathrm{w}} = 9.192\,631\,770\,\mathrm{GHz}$ folded back onto the free spectral range.

The parameters for the filter cavity are chosen as the design specifications of the Evacuable Cavity and can be seen in Table 1.

2.3 Cavity Filtering

The concept of the frequency filtering in the cavity builds on the results from section 2.1 on cavity resonances. According to (7) and (9) only light close to resonance of the cavity is transmitted, and how close depends on the cavity finesse. The shift of higher order transversal modes supplement this picture by introducing resonances in between the two Gaussian resonances as shown in section 2.2. In order to effectively filter out a desired frequency it needs to fall between mode resonances.

Because the resonance of the cavity depends not only on the frequency, but also on which cavity mode is coupled to, it is required to know how much power goes into the different modes. If the mode matching (see Appendix A) and alignment are perfect, only the Gaussian mode is excited. However this is difficult to achieve, and it is necessary to know if the cavity will be filtering sufficiently for a realistic incoupling. The power distribution on the cavity modes is calculated by the mode overlap integrals [Damask, p. 242]

$$\eta_{lm} = \frac{\left|\int E_{\mathrm{b}}^{*} E_{lm} dA\right|^2}{\int |E_{\mathrm{b}}|^2 dA \int |E_{lm}|^2 dA}, \tag{25}$$

where E_{b}, E_{lm} are the electric field of the incoming beam and the lm'th cavity mode, respectively, and take the form of (20). η_{lm} is the fraction of the power of the incoming beam that goes into the lm'th mode of the cavity. The denominator acts as normalization and in mathematical terms (25) is the expansion of the incoming beam onto the cavity eigenmodes basis. The integration is over the whole plane perpendicular to the propagation direction, and η_{lm} is independent of position.

Assuming perfect alignment the x and y integrals can be separated because the optical axis, z, of the beam and cavity modes overlap. Left is then the mode matching of waist size and position:

$$\eta_{lm} \propto \left| \int_{-\infty}^{\infty} dx\, H_l \left(\frac{\sqrt{2}x}{w_{\text{cav}}(0)} \right) e^{-\beta x^2} \int_{-\infty}^{\infty} dy\, H_m \left(\frac{\sqrt{2}y}{w_{\text{cav}}(0)} \right) e^{-\beta y^2} \right|^2 , \tag{26}$$

$$\beta = \left(\frac{1}{w_{\text{cav}}(0)} + \frac{1}{w_{\text{b}}(z')} - i \frac{k}{2R(z')} \right) . \tag{27}$$

For simplicity the integral is carried out at the waist position of the cavity modes, and z' is the waist position of the incoming beam mode. $w_{\text{b}}, w_{\text{cav}}$ is the waist size the beam and cavity modes, respectively. The assumption of perfect alignment is chosen for simplicity and from the experimental experience that it is easier to align the optical axes than to have waist match using a telescope.

From the power distribution on the cavity eigenmodes, it is possible to calculate the transmission of each mode, T_{lm}, by knowing the resonance frequency of the particular mode from (24) and the transmission from (7) and (9).

The filter ratio, ξ, is here defined as the ratio of the transmitted power to the incoming beam power

$$\xi \equiv \frac{P_{\text{t}}}{P_{\text{in}}} = \frac{\int \left| \sum_{l,m} \sqrt{T_{lm}} E_{lm} \right|^2 dA}{\int \left| \sum_{l,m} E_{lm} \right|^2 dA} = \frac{\sum_{l,m} T_{lm} \int |E_{lm}|^2 dA}{\sum_{l,m} \int |E_{lm}|^2 dA} \equiv \frac{\sum_{l,m} T_{lm} P_{lm}}{\sum_{l,m} P_{lm}} , \tag{28}$$

where the third identity holds because of the orthogonality of the Hermite polynomials, [Riley & Hobson, p. 371]:

$$\int_{-\infty}^{\infty} H_m(x) H_n(x) e^{-x^2}\, \mathrm{d}x = \sqrt{\pi} 2^n n! \delta_{nm}. \tag{29}$$

3 Experimental Setup

The idea of the laser system is to output a narrowband light beam slightly detuned with respect to the caesium D_2 transition ($\lambda = 852.2\,\text{nm}$ in air, [ASD]). Figure 6 sketches the setup of the laser system. The free running wavelength of the laser diode is not exactly as desired, and frequency pulling is needed. This is obtained via optical feedback from a diffraction grating. The first order reflection of the grating is fed back into the diode, and by varying the grating angle the frequency can be pulled to the desired. Adjustments can be made by changing temperature and diode current.

To obtain a small linewidth of the collective laser system output the laser diode is locked to a high-finesse cavity. The lock operates through optical feedback controlled by the error signal of a Hänsch-Couillaud lock (see appendices B and C). The lock actively adjusts the length of the resonator formed by the optical feedback mirror and the laser diode itself thereby keeping the light resonant with the triangular cavity.

The laser system setup includes an optical fiber for practical purposes. Though its presence requires both coupling into the fiber and from fiber to cavity (both causing power losses as mode matching is imperfect), the fiber enables quick and simple switching between different cavities. Because two different cavities are used and compared this option was chosen to ease experimental work.

The use of two different cavities is motivated by improvement. One cavity was already present at the beginning of the project, the so-called Table Top Cavity because it is mounted directly on the optics table. The other is a new design idea and will here be named Evacuable Cavity because it is mounted inside a vacuum chamber. However, evacuation was not used during the project due

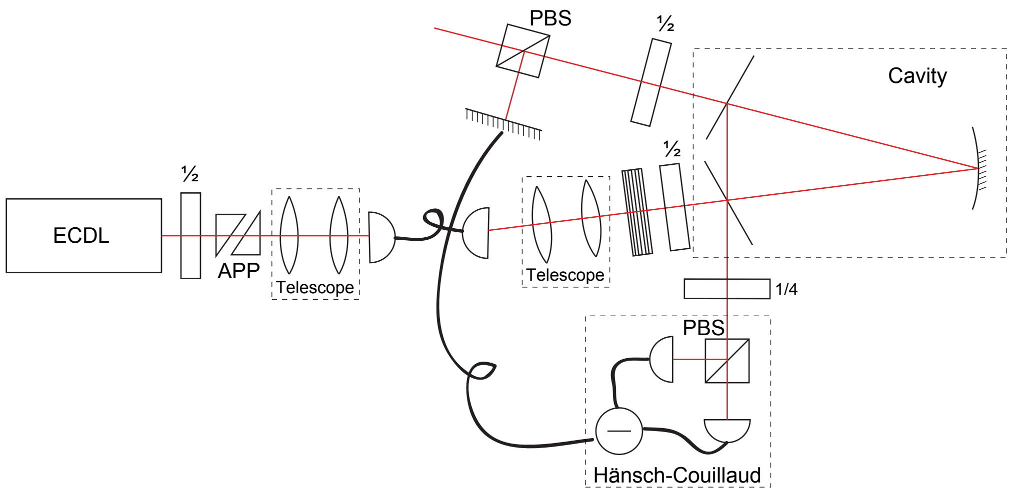

Figure 6: Sketch of laser system. Starting from left: An ECDL (Extended Cavity Diode Laser) generates the light. The ECDL is temperature controlled, includes a diffraction grating for frequency pulling, and the output beam is collimated. The beam is coupled to a single mode fiber through a system of a half-wave plate, anamorphic prism pair and a telescope. The half-wave plate optimizes transmission through the anamorphic prism pair. The output of the fiber is coupled to a triangular cavity through a telescope, polarizer and a half-wave plate – the later two to control the error signal strength. The cavity consists of two flat mirrors close to each other and a curved mirror much further away. A piezo on the back of the curved mirror allows round trip length fine tuning. The reflection of the cavity goes to a Hänsch-Couillaud lock consisting of a quarter-wave plate, polarizing beam splitter and a differential photodiode (see Appendix C). The transmission of the cavity is split by a polarizing beam splitter. One part is the output of the collective laser system the other part is fed back to the laser diode through cavity and fiber by a piezo controlled mirror. The error signal from the Hänsch-Couillaud lock controls the piezo voltage in order to lock the laser to the cavity.

to time limitations. Both cavities are triangular as the one treated in section 2. The cavities use identical mirrors from the same manufacturer but have different geometries, see Table 1.

From earlier measurements it is suspected that the Table Top Cavity is too unstable to function as locking cavity for the laser because it will not narrow down the laser linewidth sufficiently. In the experimental work presented here the Table Top Cavity will mainly function as locking cavity to do better measurements on the Evacuable Cavity and for comparison.

3.1 Measurement Methods

The work presented in this report includes measurements of the following characteristic features of the laser system:

1. **Photon Lifetime in the Evacuable Cavity**
   Method: Ring-down. By amplitude modulation of the current through the laser diode sidebands are created on the output light. The cavity round trip length is adjusted to accommodate the frequency of one of the sidebands by changing the voltage over the piezo behind the curved cavity mirror. A fast photodiode measures the transmitted light from the cavity.
   The modulation is turned on and off at a frequency much lower than the modulation and much lower than the inverse of the photon lifetime. This is done for experimental ease. The cavity is not locked and so we wait for the cavity to drift into sideband resonance. When the sideband turns off we see the ring-down signal on an oscilloscope, and we have enough time to stop the oscilloscope trigger and save the signal.

When the modulation is applied the field builds up inside the cavity, and as it is turned off the field will decay exponentially with a characteristic photon lifetime dependent on the cavity bandwidth according to (16).
Parameters used were modulation frequency, $\nu_{\mathrm{AM}} = 12.5\,\mathrm{MHz}$ and on/off switching at 1 Hz. The modulation strength was set so that the power in the sidebands were comparable to the power in the carrier. By inserting a half-wave plate before the cavity switching between the high- and low-finesse polarization is possible.
The laser was not locked to the Table Top Cavity.

2. **Spectrum of the Evacuable Cavity**
Method: By sweeping the voltage over the piezo behind the curved cavity mirror the round trip length, and thereby the cavity resonance frequency, ν_{c}, is swept. A photodiode measures the power of the light transmitted from the cavity.
When the sweep is sufficiently long the full FSR spectrum can be seen from the time trace of the photodiode signal.
To have ν_{c} linear in time a triangle wave signal is applied to the piezo. This implies the assumption that the piezo response is linear. Note in addition that because the laser light frequency $\nu \approx 350\,\mathrm{THz}$ is huge compared to the FSR ($\approx 200\,\mathrm{MHz}$), it is only necessary to change the cavity length by an extremely small amount, and the inverse proportionality of round trip length and ν_{c} is approximately linear.
In order to see higher order modes the incoming beam is slightly misaligned to the cavity. This way the higher order modes are more strongly excited.
A polarizing beam splitter is inserted in the setup before the fiber, and the new path is coupled to a second fiber. This way the laser can be send to two cavities simultaneous. The Table Top Cavity is used to lock the laser through optical feedback controlled by the Hänsch-Couillaud lock to ensure a more narrow laser linewidth than when the laser is free running. The Evacuable Cavity can then be measured by coupling in the locked laser.
A sideband modulation is used to measure the free spectral range and calibrate the time trace of photodiode signal into frequency. The function generator that generates the modulation was not able to output a modulation with frequency close to the FSR. Instead the method was to increase the frequency until the sidebands of the higher order modes overlapped and noting the frequency.

	L	w_0	z_{R}	$\mathcal{F}$	$\delta\nu_{\mathrm{c}}$	$\Delta\nu_{\mathrm{FSR}}$
Table Top Cavity	1.10 m	660 µm	1.60 m	3413	79.8 kHz	273 MHz
Evacuable Cavity (Design specs)	1.494 05 m	695 µm	1.78 m	3413	58.8 kHz	201 MHz
Evacuable Cavity (Realized)	1.495 m $\pm$0.006 m	704.7 µm $\pm$0.6 µm	1831 mm $\pm$3 mm	$2.79 \cdot 10^3$ $\pm 0.19 \cdot 10^3$	72 kHz $\pm$5 kHz	200.5 MHz $\pm$0.8 MHz

Table 1: Cavity parameters: round trip length, waist size, Rayleigh length, finesse, bandwidth and free spectral range for the two cavities in use. Round trip length is measured for the Table Top Cavity. The rest of the parameters are calculated from the cavity length, mirror reflectivities and curvature. Both cavities use the same mirrors. In- and outcoupling mirrors are flat with 99.91% reflection for s-polarization. The curved mirror has a radius of curvature $R_{\mathrm{mirror}} = 5.000\,\mathrm{m}$ and 99.996% reflectivity for s-polarization. The numbers are provided by the manufacturer.
Realized L, w_0, z_{R} and $\mathcal{F}$ is calculated from measured FSR, bandwidth and tweaked mirror radius of curvature (section 4.2) from which measurement errors propagate.

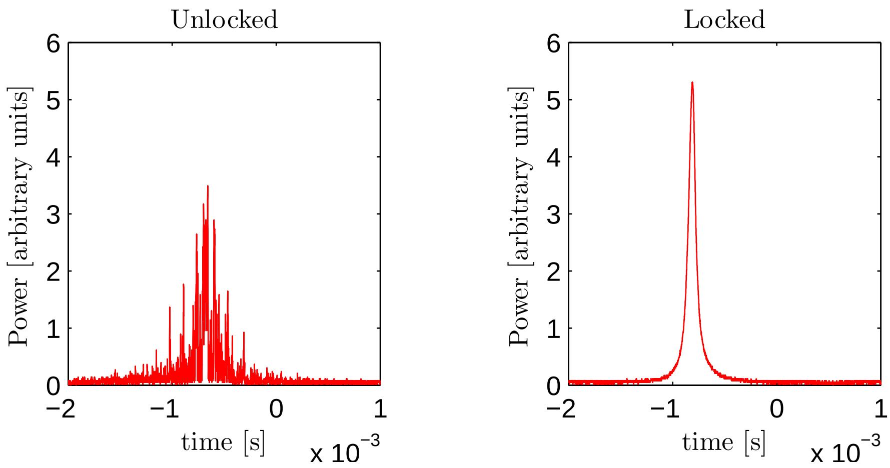

Figure 7: Cavity scans with locked and unlocked laser. The peak seen is the high-finesse 00-mode of the Evacuable Cavity. The piezo behind the curved cavity mirror is scanned to scan the cavity resonance frequency. Therefore the transmission power changes with time. The locked laser shows a much clearer peak, and this can be explained by the locked laser having a narrower linewidth and less random phase noise.

4 Experimental Results

After a couple of months work of setting up the experiment – including assembling the ECDL, pulling the frequency close to $\lambda = 852.2\,\mathrm{nm}$, collimating and shaping the beam profile with an anamorphic prism pair, coupling into a single mode fiber and plenty of other tasks new to an inexperienced optical physicist – it was possible to produce experimental results. The results together serve as a characterization of the laser system for the deterministic single photon source, and one of the first things that was clear when the system was up and running was the difference between the free running laser and the locked laser. Besides being much easier to work with because of stability the locked laser is subject to less noise from the amplified spontaneous emission the broadband gain medium introduces resulting in a narrower laser linewidth as can be seen in Figure 7.

4.1 Photon Lifetime in the Evacuable Cavity

A measurement of the cavity photon lifetime was carried out by a ring-down measurement. 16 runs were made for the high-finesse (HF) polarization and 9 for the low-finesse (LF) polarization. A plot of data from one of the runs can be seen in Figure 8. For all runs the transmitted power showed clearly exponential decay when the sidebands were turned off, and the ring-down time (i.e. the photon lifetime) was determined by the best fit to an exponential function, $ae^{t/\tau_c} + b$. The confidence bound for the fitting was extremely small in all cases and is therefore ignored. However, the determined value of τ_c varies a lot between runs, especially for the high-finesse where the values vary by up to a factor two. The mean values with the variance of the mean is:

$$\tau_c^{\mathrm{HF}} = 2.36 \pm 0.15\,\mu\mathrm{s} \;\Leftrightarrow\; \delta\nu_c^{\mathrm{HF}} = 72 \pm 5\,\mathrm{kHz}, \tag{30}$$

$$\tau_c^{\mathrm{LF}} = 119 \pm 4\,\mathrm{ns} \;\Leftrightarrow\; \delta\nu_c^{\mathrm{LF}} = 1.35 \pm 0.04\,\mathrm{MHz}. \tag{31}$$

The lowest value for any of the ring-down measurements was $\delta\nu_c^{\mathrm{HF}} = 46.1\,\mathrm{kHz}$ which is significantly below the expected. A way of explaining the variance in the photon lifetimes could be to say that extra internal cavity losses are caused by a fluctuating dust density. In this perspective it is worth considering the lowest bandwidth value, and it can be hoped that when Evacuable Cavity is evacuated this bandwidth can be achieved. It is difficult to explain from where an extra long photon lifetime could arise.

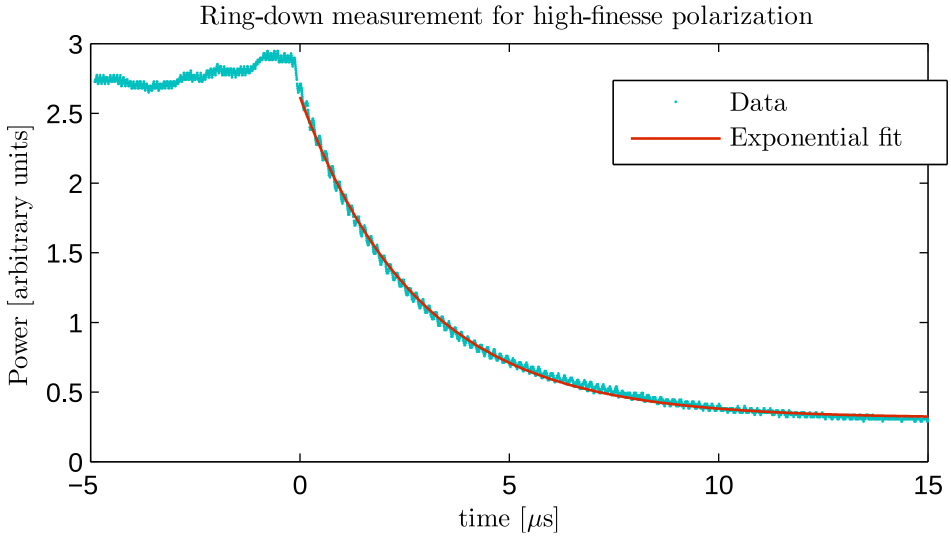

Figure 8: Ring-down measurement for high-finesse polarization. Plotted data [cyan] is a time trace of the power of transmitted light from the cavity at resonance with a sideband of frequency 12.5 MHz. At time $t = 0$ the sideband is turned off, and the cavity field decays. An exponential fit, $ae^{t/\tau_c}+b$, of the ring-down decay [orange] determines the photon lifetime $\tau_c = 2.84\,\mu s$ corresponding to a cavity bandwidth $\delta\nu_c = 56.0\,\text{kHz}$. An oscillation of approximately 6.25 MHz is present on the ring-down.

Two more comments should be added to experimental data from the ring-down measurement: 1) The power of the transmitted light before the sideband modulation is turned off varies significantly between runs. The ratio of the most powerful to the least is approximately 200 for the high-finesse runs. This questions how well the sideband was coupled in to the cavity, and if in some runs it was the second sideband (twice the frequency difference with the carrier) which was measured. 2) All runs show an oscillation on the transmission power, particularly strong for the low-finesse polarization. This effect can be seen in Figure 8. An investigation shows that when the sidebands are on, $t < 0$, the oscillation frequency is 12.5 MHz for all runs which can be explained by a bit of the carrier being coupled in resulting in a beat note with the sideband. Because the low-finesse polarization has a broader bandwidth more of the carrier will be coupled in, and the beat note becomes stronger. For $t > 0$ the oscillation frequency is different and varies between runs. Some show the 12.5 MHz oscillation on the ring-down while others show integer fractions of 12.5 MHz.

Both of the mentioned varying features for the transmission signal was compared to the value for the photon lifetime, τ_c, to look for a possible systematic connection, but no connection between photon lifetime and sideband power nor ring-down oscillation frequency was found.

4.2 Evacuable Cavity Spectrum

The cavity spectrum was measured with the laser locked to the table top cavity. A plot of the spectrum for the full FSR can be seen in Figure 9. The spectrum shows a high degree of compliance with theoretically predicted spectrum in Figure 5 on several accounts. First to notice is that the separation of the modes of the same polarization is approximately one eighth of the FSR. Furthermore in the vicinity of the 00-mode two higher order modes are seen with equal separation, see Figure 10 for a close up. This is as expected for the 13- and 08-modes where according to (24) the separation from the 00-mode is, respectively, $\Delta\phi_{13} = 4\alpha + \pi$ for the odd l mode and $\Delta\phi_{08} = 8\alpha$ for the even l mode when $\alpha \neq \frac{\pi}{4}$.

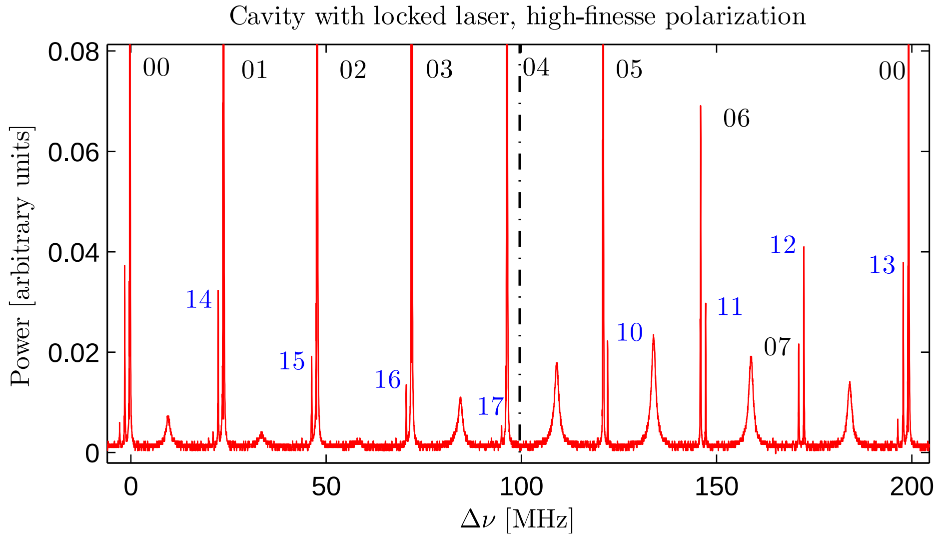

Figure 9: Free spectral range (FSR) cavity spectrum with locked laser in high-finesse polarization. First peak is the 00-mode, and last peak is the same mode one FSR away. The FSR is $\Delta\nu_{\mathrm{FSR}} = 200.5{\pm}0.8\,\mathrm{MHz}$. The dotted line mark half the FSR. The incoming beam is intentionally misaligned to excite the higher order modes, and the vertical higher order modes are excited stronger than the horizontal modes because the misalignment was along the vertical axis. The wide peaks are low-finesse polarization that appears due to imperfect polarizing of the laser beam. The frequency axis is introduced according to the FSR measurement.

The high-finesse polarized modes show the expected behaviour derived in section 2.2 appearing in pairs eight divisions along the FSR. The mode separation is $24.74 \pm 0.1\,\mathrm{MHz}$. The low-finesse polarized modes were expected to be resonant at the same frequencies as the HF modes, evidently they appear in between the HF modes. This might prove to be a calamitous challenge for filtering capabilities of the cavity if they are not sufficiently suppressed.

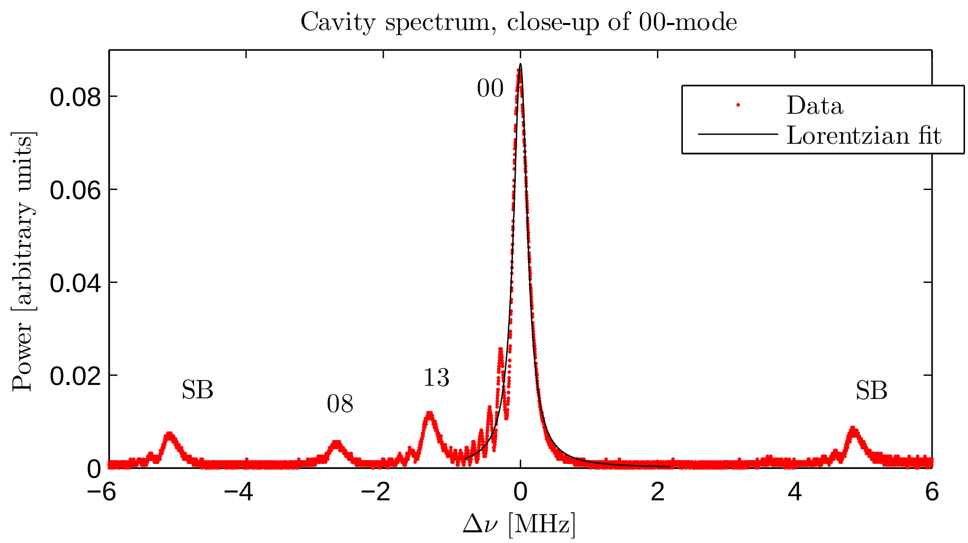

Figure 10: Close-up of the high-finesse 00-mode in the Evacuable Cavity with sidebands for calibration. The two outer peaks are the sidebands of 5 MHz. Second peak from the left is the 08-mode, third peak is the 13-mode, and frequencies are measured with respect to the largest peak – the 00-mode. The separation of the 08- and 00-mode is $\delta\nu_{08} = 2.58 \pm 0.1\,\mathrm{MHz}$.

The Lorenztian fit gives an upper estimate for the linewidth of the locked laser of 250 kHz.

By introducing sidebands as calibration the separations were measured to be:

$$\Delta\nu_{13} = \frac{(4\alpha+\pi)}{2\pi}\Delta\nu_{\mathrm{FSR}} = 1.27 \pm 0.1\,\mathrm{MHz}, \tag{32}$$

$$\Delta\nu_{08} = \frac{(8\alpha)}{2\pi}\Delta\nu_{\mathrm{FSR}} = 2.58 \pm 0.1\,\mathrm{MHz}. \tag{33}$$

With a camera behind the curved cavity mirror it was possible to identify the modes as the two mentioned (photos can be seen in Appendix D). The rest of the HF peaks appear in pairs (i.e. slightly separated with a spacing equivalent to the separation of the 13- and 08-modes) and was also identified as the expected modes.

The mode separation, $\Delta\nu_{\mathrm{TEM}} = \alpha/(2\pi)\cdot\Delta\nu_{\mathrm{FSR}}$, was measured by overlapping sidebands of two adjacent modes and determined to be: $\Delta\nu_{\mathrm{TEM}} = 24.74 \pm 0.1\,\mathrm{MHz}$. Together with $\Delta\nu_{08}$ this gives a measure for the cavity FSR:

$$\Delta\nu_{\mathrm{FSR}} = 8\Delta\nu_{\mathrm{TEM}} + \Delta\nu_{08} = 200.5 \pm 0.8\,\mathrm{MHz}, \tag{34}$$

which is consistent with the expected value 201 MHz and shows that the realized cavity round trip length agrees with the design specifications.

In the theoretically predicted spectrum the mode separation is calculated from cavity length and mirror curvature cf. (24), and eight separations are a little *more* than the FSR, cf. Figure 5. The experimental spectrum shows however that the realized separation is a little *less* than one eighth of the FSR. This leads to suspecting the mirror curvature does not meet the manufacturer data. We suspect that a change in the mirror curvature is introduced by clamping the mirror and compressing it with the piezo. However, with our limited range on piezo expansion it was not possible to determine an unambiguous change in the curvature by looking for a change in the mode separation, $\Delta\nu_{\mathrm{TEM}}$. To fit the measured mode separation the *de facto* mirror radius of curvature would have to be $R_{\mathrm{mirror}} = 5.23\,\mathrm{m}$ which we consider a significant deviation from the stated 5.000 m.

From the close-up of the 00-mode in Figure 10 it is possible to extract information of the locked laser linewidth, $\delta\nu$. A fit to a Lorentzian function, $a\cdot\delta\nu/[2(\Delta\nu^2+(\delta\nu/2)^2)]+b$, yields $\delta\nu = 250\,\mathrm{kHz}$ which should be considered an upper estimate for the linewidth. The value is much bigger than the cavity bandwidth from the ring-down measurement, and it is reasonable to assume that the peak width seen is primarily caused by the laser linewidth. However, what cannot be seen in the figure is the time duration for the measurement. Time goes from right to left in this case, and the time from the 00-mode peak to the next peak is approximately 15 µs which is very close to the photon lifetime. Therefore it might just be the ring-down we are seeing, and 250 kHz becomes no more than an upper estimate. The oscillations present on the left slope (i.e as the cavity goes *out* of resonance) are also consistent with the frequency scan being too fast because it reassembles the behaviour theoretically predicted in [Morville et al.] for a fast frequency scan. Determining the locked laser linewidth will require further measurements.

The experimental spectrum shows further that the locked laser beam contains low-finesse polarized light and that this light is resonant at frequencies between the HF resonance frequencies. From (24) the LF modes should be shifted by half an FSR making them resonant for same frequencies as the odd l HF modes, but the experimental spectrum shows that the LF modes acquires an additional phase of $\phi_{\mathrm{LF}} = 0.529\alpha \pm 0.01\alpha$. By inspection of a similar spectrum for the Table Top Cavity it was verified that the relative position of the LF 00-mode is identical. Since the two cavities consist of identical mirrors we conclude that the extra acquired phase is a property of the mirrors, and we suspect that it comes from the in- and outcoupling mirrors where the angle of incidence is large and could introduce a polarization dependent effect.

This effect is very disturbing for the filtering capabilities of the cavity as it was designed such that excitation light with a frequency 9.192 631 770 GHz away from the resonant mode and a different polarization would fall between peaks and thus be filtered out. If instead the excitation light is actually resonant (or at least a higher order is resonant), it would require an almost perfect mode matching to filter out that light.

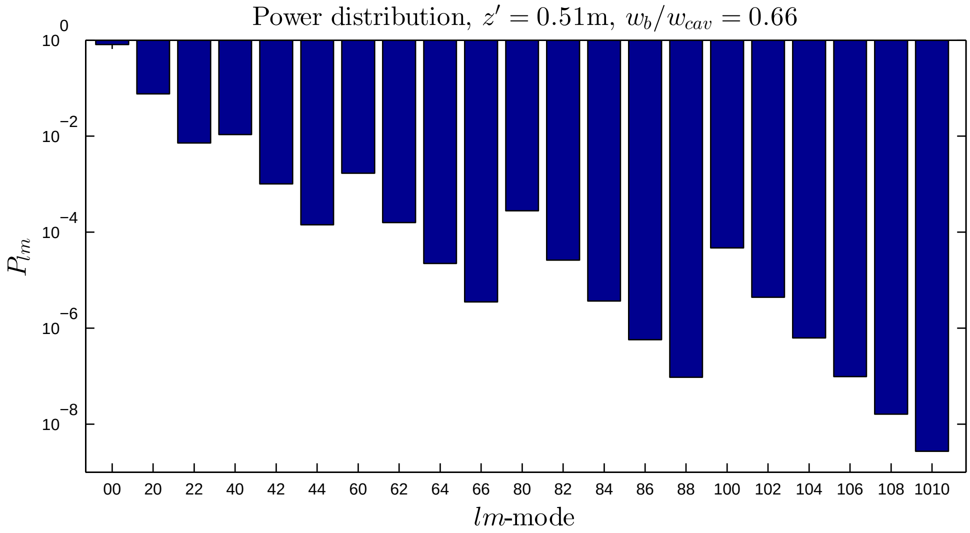

Figure 11: Calculated power distribution on higher order modes for configuration (c). The lm'th mode power, P_{lm}, is normalized to incoming beam power. The ratio of the beam waist size to the cavity waist size is $w_{\mathrm{b}}/w_{\mathrm{cav}} = 0.66$, and the waist position offset is $z' = 0.51$ m. The overlap with the higher order modes comes from waist size and position mismatch and is therefore symmetric in the horizontal and vertical modes. Only one is shown.

5 Filter Ratio Calculation

In the full setup of the single photon source it will be necessary to filter out a single photon from a stronger field (10^9 photons), both to detect the heralding photon that signals that a photon is stored in the Cs-cell and to output the single photon. In both cases the photon is emitted into the same spatial mode as the excitation light but in the perpendicular polarization. Therefore the filter process consists of first a polarizing beam splitter and afterwards a filter cavity. This section describes the calculation of the frequency filtering from the filter cavity.

In the write process the heralding single photon will be separated from the excitation pulse by the frequency $\delta\nu_{\mathrm{w}} = 9.192\,631\,770\,\mathrm{GHz}$ which is the transition of a Cs atom that defines the second [BIPM]. The filter cavity will be configured to be on resonance with the single photon, and the design of the cavity ensures that the excitation pulse is not resonant for any of the lowest order transversal modes to allow for imperfect incoupling (resonance of these modes are treated in section 2.2). The parameters for the filter cavity are chosen as the corrected parameters of the Evacuable Cavity and can be seen in Table 1. The cavity is designed to have a separation of modes slightly different than one eighth of the free spectral range. This way the higher order modes are not resonant on the exact same frequency of the 00-mode, and only very high order modes are resonant with the frequency of the excitation pulse. It is the hope that the corrections to the cavity length does not change this significantly.

To calculate filter ratio of the cavity we use a MATLAB-script (see Appendix E). First the script calculates power distribution on the higher order modes by solving the mode overlap integral (25) analytically – exploiting separability of the x and y axes. An example of the power distribution is shown in Figure 11. Next, the transmittance of the different modes is calculated

Configuration	ξ^{LF}	ξ^{HF}	P_{00}	P_{higher}
(a)	$0.236 \cdot 10^{-6}$	$203 \cdot 10^{-6}$	1	0
(b)	$0.274 \cdot 10^{-6}$	$516 \cdot 10^{-6}$	0.81	$0.121 \cdot 10^{-6}$
(c)	$0.274 \cdot 10^{-6}$	$515 \cdot 10^{-6}$	0.81	$0.119 \cdot 10^{-6}$

Table 2: Result of filter ratio calculation for three configurations: a) perfect mode match, b) both lenses 10 mm too close to each other and c) both lenses 10 mm too far from each other. ξ^{LF} is the filter ratio for the single photon in low-finesse polarization and ξ^{HF} for high-finesse polarization. The excitation beam is in the opposite polarization in both cases. P_{00} is the power in the 00-mode, and P_{higher} is the total power in the modes above the cut-off mode. The latest two normalized to incoming beam power.

from (7) and (9) using the resonance conditions in (24):

$$T_{lm}^{\mathrm{LF}} = T_{\max} \left[1 + F \cos^2 \left(\frac{\phi_{\mathrm{w}} - \phi_{\mathrm{LF}} - (l+m)\alpha - \left(1 - (-1)^l\right) \frac{\pi}{2}}{2} \right) \right]^{-1}, \tag{35}$$

$$\phi_{\mathrm{w}} = 2\pi \frac{\delta\nu_{\mathrm{w}}}{\Delta\nu_{\mathrm{FSR}}}, \tag{36}$$

where $\Delta\nu_{\mathrm{FSR}}$ is the free spectral range, and ϕ_{LF} is the phase shift of LF modes found in section 4.2. T_{lm}^{LF} is the transmittance of the excitation beam in LF polarization when the cavity is resonant with the single photon in HF polarization. The filter ratio is then calculated using (28).

In the full single photon source setup the excitation beam will come from the Science Cavity (see section 1.1), but since this is not yet built the following will use a beam from the fiber used in the current setup. The incoming beam is assumed to be a 00-mode since it comes from a single mode fiber, and before entering the cavity the beam goes through a telescope in order to match the cavity eigenmodes. The cavity eigenmodes are determined from the geometry of the cavity, and the output beam of the fiber is measured with a 'waist meter' to determine the beam waist size and position, see Appendix A.

The scope of the script is to vary the telescope configuration (i.e. slightly changing the position of the two lenses) and calculate how much power of the excitation pulse is transmitted. The choice of varying the telescope and not the beam alignment is made from the assumption that alignment is easier to optimize as it can be fine tuned with mirrors while looking at the live transmission signal. The script operates with three configurations: a) perfect mode match, b) both lenses 10 mm too close to each other and c) both lenses 10 mm too far from each other. This way an upper bound on mode mismatch is estimated as it should be possible to place the lenses within a 10 mm accuracy.

The calculation goes up to a certain order of cavity modes, and the total power coupled into the modes higher than this cut-off mode, P_{higher}, is calculated. The choice of cut-off mode is determined from P_{higher} and was set to the (16,16)'th mode. The result from the calculation of the filter ratio is shown in Table 2.

6 Discussion of Results

The result from the cavity ring-down measurement showing a cavity bandwidth of $\delta\nu_{\mathrm{c}}^{\mathrm{HF}} = 72 \pm 5$ kHz for the high-finesse polarization of the Evacuable Cavity requires some considerations. The value should be compared to the expectation from the theoretical considerations in (12) where the finesse is estimated from the mirror reflectivity values specified by the manufacturer. The expected value is for the high-finesse polarization $\delta\nu_{\mathrm{c}}^{\mathrm{HF}} = 58.8$ kHz, and mirror reflectivities for the low-finesse polarization is not stated by the manufacturer. The experimental value for $\delta\nu_{\mathrm{c}}^{\mathrm{HF}}$ is a little more than two standard deviations away from the expected bandwidth, but that the bandwidth is broader than the calculated value is not surprising. The cavity round trip length may deviate slightly from the design in either directions without a significant impact on the bandwidth, but the main concern is the losses inside the cavity that are not accounted for by the mirror reflectivities, for instance surface scattering or clipping at the mirrors. That the experimental result does not deviate more than 20% from loss-free calculations can be considered satisfactory and shows that losses are not a significant problem for the cavity.

Though the cavity bandwidth is relevant for the filter ratio calculation it cannot stand alone as a characterization of the laser system. First of all it is necessary to determine the linewidth of the laser when it is locked to the cavity to know that it will function as a laser source for the single photon source. It is not given that the locked laser will achieve the same linewidth as the bandwidth of the cavity to which it is locked. This requires further investigations and measurements.

Secondly, it is not sufficient to have a narrow laser linewidth. The laser is also required to be frequency stable with respect to the filter cavity. To determine the laser stability will also require further investigation. A potential way to proceed on both laser linewidth and stability would be to beat the locked laser against another relatively stable laser and from that signal determine the relative stability and linewidth.

A third and related concern is the presence of mode jumps. Even with the laser locked to the Table Top Cavity we experienced jumps in the frequency which we associate with mode jumps in the laser diode. The jumping rate depends strongly on the current through the diode and the power of the optical feedback. If the optical feedback is too strong, the laser will go into a state where it is extremely noisy and exhibit mode jumps continuously. The same behaviour is seen for certain current regions. Working with the laser we have learned what configuration are more suitable than others, but the 'magic' setting is still to be found.

The results from the filter ratio calculation shown in Table 2 are encouraging regarding the future use of the Evacuable Cavity for filtering out the excitation beam from the heralding single photon. In particular if the system is configured to have the single photon in the low-finesse polarization of the cavity, the transmitted power of the excitation beam – which is in the opposite polarization – will be satisfactorily below the required 10^{-4}. The calculation also shows that for this polarization configuration the filter ratio is not sensitive to the mode matching within the limits of laboratory realization.

There is however a strong limitation to the reliability of the calculation result. The model does not take account of a possible misalignment of the optical axes of the incoming beam and cavity which will cause excitation of the antisymmetric cavity modes. These were regarded fairly suppressible, but in the light of the cavity spectrum analysis they will require further attention. The cavity spectrum analysis revealed two important properties: 1) A phase shift for the low-finesse polarization which was not expected from theoretical approach. 2) A different mode spacing than expected from the design specifications. Both modifications were incorporated in the filter ratio calculation model, but in particular the first will have a significance for the filtering of antisymmetric cavity modes – especially if some of the excitation beam leaks into the same polarization as the single photon.

Therefore the next step will be to expand the filter ratio script to include misalignment of the optical axes, and the preliminary results justifies continuing the work on the Evacuable Cavity as the filter cavity. Further more there is still the expectation that evacuation will improve the cavity performance.

7 Conclusion

By assembling an extended cavity diode laser and locking it to an external triangular cavity a second triangular cavity has been analysed. The bandwidth of the cavity was found to be $\delta\nu_{\mathrm{c}}^{\mathrm{HF}} = 72 \pm 5\,\mathrm{kHz}$ which is only 20% higher than expected from the mirror specification. On that ground it is concluded that internal cavity losses are not a substantial challenge for the cavity.

A theoretical approach to the triangular cavity has shown that the cavity is expected to have frequency filtering properties that are sensitive to the polarization and horizontal symmetry of the cavity modes as oppose to the more common standing wave cavity. The properties have been verified by a cavity spectrum analysis where the free spectral range was determined as $\Delta\nu_{\mathrm{FSR}} = 200.5 \pm 0.8\,\mathrm{MHz}$ and the mode spacing as $\Delta\nu_{\mathrm{TEM}} = 24.74 \pm 0.1\,\mathrm{MHz}$. The spectrum analysis also showed an unexpected phase shift for the low-finesse polarization of 52.9% ± 1% of the phase-wise mode spacing.

The determined filter cavity characteristics were incorporated in a calculation of the cavity filter ratio resulting in a transmission coefficient for the excitation beam $\xi^{\mathrm{LF}} < 0.3 \cdot 10^{-6}$ for feasible mode matching and with the cavity resonant with the single photon in low-finesse polarization.

In total the determined cavity properties and its expected filtering capabilities leads to recommending a continued investigation of the cavity as a candidate for the filter cavity in the full single photon setup.

Acknowledgements

The results presented in this thesis are the outcome of laboratory work conducted in the period from February 2014 to June same year. As a novice in the field of experimental optical physics I am aware that this could not have been done without the help from more experienced people whom I would like to mention. I thank Eugene Polzik for giving me the privileged opportunity to be a part of QUANTOP, for welcoming me in the team and for supervising the project. I would also like to give thanks to Jürgen Appel, Jörg Müller and the rest of the laboratory staff for giving me numerous advices and being ready for discussions.

Finally, I am especially grateful to Michael Zugenmaier who let me in on the single photon source experiment, taught me all the tricks for working with optics and had an amazing patience when things had to be explained yet another time. Thank you.

References

[ASD] Kramida, A., Ralchenko, Yu., Reader, J., and NIST ASD Team (2013). ”NIST Atomic Spectra Database (ver. 5.1)”, [Online]. Available: `http://physics.nist.gov/asd` [2014, May 25]. National Institute of Standards and Technology, Maryland, USA.

[BIPM] ”Unit of time (second)”, [Online]. Available: `http://www.bipm.org/en/si/base_units/second.html` [2014, May 28]. Bureau International des Poids et Mesures, France.

[Damask] J. N. Damask, ”Polarization Optics in Telecommunications”, Springer Science+Business Media, Inc., New York, USA (2005)

[DLCZ] L.-M. Duan, M.D. Lukin, J.I. Cirac, and P. Zoller, ”Long-distance quantum communication with atomic ensembles and linear optics”, Nature 414, 413 (2001).

[Dudin et al.] Y. O. Dudin, L. Li, and A. Kuzmich, ”Light storage on the time scale of a minute”, Phys. Rev. A 87, 031801(R) (2013)

[Higgimbottom et al.] D. B. Higginbottom, B. M. Sparkes, M. Rancic, O. Pinel, M. Hosseini, P. K. Lam, and B. C. Buchler, ”Spatial mode storage in a gradient echo memory”, Phys. Rev. A 86, 023801 (2012)

[Hänsch & Couillaud] T. W. Hänsch and B. Couillaud, ”Laser frequency stabilization by polarization spectroscopy of a reflecting reference cavity”, Opt. Commun. 35, 441 (1980)

[ing.dk] ”Teleportation er årets bedste danske forskningsresultat”, [Online]. Available: `http://ing.dk/artikel/teleportation-er-aarets-bedste-danske-forskningsresultat-164942` [2014, June 3]. Mediehuset Ingeniøren A/S, Denmark

[Knill et al.] E. Knill, R. Laflamme, and G. J. Milburn, ”A scheme for efficient quantum computation with linear optics”, Nature 409, 46 (2001)

[Kogelnik & Li] H. Kogelnik and T. Li, ”Laser Beams and Resonators,” Appl. Opt. 5, 1550 (1966)

[Ladd et al.] T. D. Ladd, F. Jelezko, R. Laflamme, Y. Nakamura, C. Monroe and J. L. O'Brien, ”Quantum computers”, Nature 464, 45 (2010)

[Lloyd] S. Lloyd, ”Universal quantum simulators”. Science 273, 1073 (1996).

[Lvovsky et al.] A. I. Lvovsky, B. C. Sanders and W. Tittel, ”Optical quantum memory”, Nature Photonics 3, 706 (2009)

[Milonni & Eberly] P. W. Milonni and J. H. Eberly, ”Laser Physics”, John Wiley & Sons, Inc., Hoboken, New Jersey (2010)

[Morville et al.] J. Morville, D. Romanini, M. Chenevier and A. Kachanov, ”Effects of laser phase noise on the injection of a high-finesse cavity”, Appl. Opt. 41, 6980 (2002)

[Petersen] J. M. Petersen, ”An Ion Crystal Quantum Repeater”, Master thesis, University of Copenhagen (2010)

[Riley & Hobson] K. Riley and M. Hobson, ”Essential Mathematical Methods for the Physical Sciences”, Cambridge University Press, United Kingdom (2011)

[Thorlabs] ”Glan-Thompson Polarizers”, [Online]. Available: `http://www.thorlabs.de/newgrouppage9.cfm?objectgroup_id=116` [2014, June 10]. Thorlabs Inc., New Jersey, USA.

[Tkack & Chraplyvy] R. W. Tkack and A. R. Chraplyvy, ”Regimes of Feedback Effects in 1.5-µm Distributed Feedback Lasers”, Journal of Lightwave Technology 4, 1655 (1986)

[Zhao, Chen et al.] B. Zhao, Y.-A. Chen, X.-H. Bao, T. Strassel, C.-S. Chuu, X.-M. Jin, J. Schmiedmayer, Z.-S. Yuan, S. Chen and J.-W. Pan, ”A millisecond quantum memory for scalable quantum networks”, Nature Physics 5, 95 (2009)

Appendices

A Mode Matching

To couple light into a structure (e.g. fiber or cavity) the incoming beam will have to match the mode of the structure. A beam front is characterized by the radius, $w(z)$, and the radius of curvature, $R(z)$, [Kogelnik & Li]. Both can be expressed through the beam parameter $q(z) = z + iz_{\mathrm{R}}$ using the relations written below (21). The evolution of q through optical elements can be written on matrix formula according to [Kogelnik & Li]:

$$\begin{pmatrix} \lambda q' \\ \lambda \end{pmatrix} = \begin{pmatrix} A & B \\ C & D \end{pmatrix} \begin{pmatrix} q \\ 1 \end{pmatrix}. \tag{37}$$

In the presented work mode matching has mainly involved setting up telescopes with two lenses. Here two ABCD-matrices are of interest: 1) free space propagation and 2)lens of focal length, f. The matrices are according to [Kogelnik & Li]:

$$\begin{pmatrix} 1 & z \\ 0 & 1 \end{pmatrix} \quad , \quad \begin{pmatrix} 1 & 0 \\ \frac{-1}{f} & 1 \end{pmatrix}. \tag{38}$$

That means for a telescope of two lenses that the corresponding equation is:

$$\begin{pmatrix} \lambda q' \\ \lambda \end{pmatrix} = \begin{pmatrix} 1 & 0 \\ \frac{-1}{f_2} & 1 \end{pmatrix} \begin{pmatrix} 1 & d \\ 0 & 1 \end{pmatrix} \begin{pmatrix} 1 & 0 \\ \frac{-1}{f_1} & 1 \end{pmatrix} \begin{pmatrix} q \\ 1 \end{pmatrix}, \tag{39}$$

where d is the interlens distance. When the beam parameter for the incoming beam and for the target structure is known, a suitable choice of lens configuration can be found from (39).

To couple to the fiber in the experimental setup the first thing was to determine the beam parameter for the laser beam. This was done by using a waist meter to measure the beam radius at several positions along the propagation direction and fitting to $w(z) = w_0^2 \left[1 + (z/z_{\mathrm{R}})^2\right]$, [Kogelnik & Li]. The same measurement is done for the fiber by coupling light in and measuring the output beam from the other end. Figure 12 shows the fiber output.

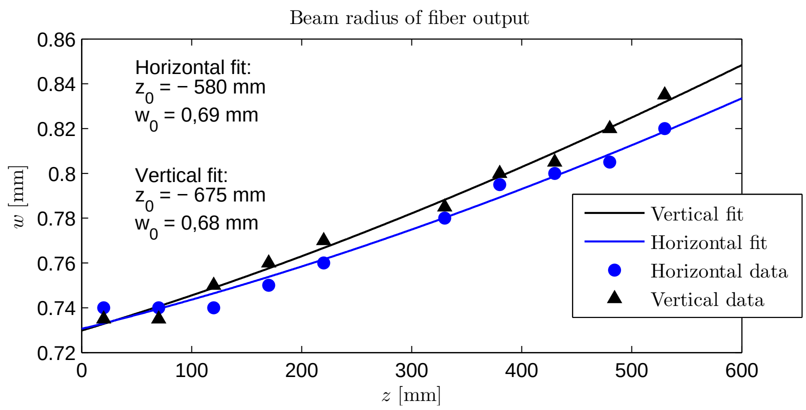

Figure 12: Beam radius for the fiber output for determining the beam parameter q. The beam radius was measured both along the horizontal and vertical axes. z is the distance from the fiber outcoupler. The fit to the vertical data showed the best goodness of fit and was chosen for the mode matching calculation.

B Table Top Cavity Transmission and Optical Feedback

A way to narrow down a laser linewidth is optically feeding back the laser light into the laser diode, but the diode behaviour varies with the power that is fed back, including unwanted behaviour such as mode jumping [Tkack & Chraplyvy]. Therefore it is relevant to have an idea of the power sent back to the diode when locking the laser to the Table Top Cavity. This we also want to compare with the capture range, i.e. the frequency range for which the laser can be pulled to cavity resonance. The method used is similar to the cavity spectrum measurement. The Table Top Cavity was scanned but without locking the laser. The power is measured at three positions simultaneously using three photodiodes. The transmission, P_t, is measured at the output after the cavity. The feedback power is measured at two positions: 1) behind the partly transmitting feedback mirror, P_m, and 2) on the same side of the cavity as the laser, P_f, by inserting a 50/50 beam splitter between the fiber and the polarizer. photodiodes were calibrated using a power meter, and the error bars come from the calibration uncertainty. 10 measurements were done with increasing feedback strength. Figure 13 shows measurement data.

To compare the powers of different measurements the highest peak values are plotted against each other in Figure 14. They show that the coupling back through the cavity is inefficient. The best measured ratio of the P_f to P_m is 20%. The feedback mirror has a 70% reflectivity meaning that 30% is measured in P_m, and only half of the feedback power on the laser side of the cavity is measured in P_f because of the beam splitter. This means that ideally the ratio of the measured should be $P_\mathrm{f}/P_\mathrm{m} = 70\%/30\% \cdot 50\% = 117\%$.

The capture range is measured as the time from the rise slope of the first 00-mode peak to the down slope of the last, but the measurement is ambiguous because it is difficult to determine which peaks are 00-modes and not higher order modes. The best way to estimate this is to look at the peak height. Capture range values are rather discretionary since when the feedback power reaches a certain level a new peak will arise and one more for even higher power, etc. The measured values are shown in Figure 15. The capture range does go up for higher feedback power, but it is difficult see a clear relation. For the highest powers the capture range is almost the full FSR, but here the diode tend to become unstable making frequent mode jumps. From experience the optimal feedback power P_f is around 1-2 µW as the situation in Figure 13. Here the Hänsch-Couillaud Lock can lock the laser on the time scale of minutes up to around half an hour.

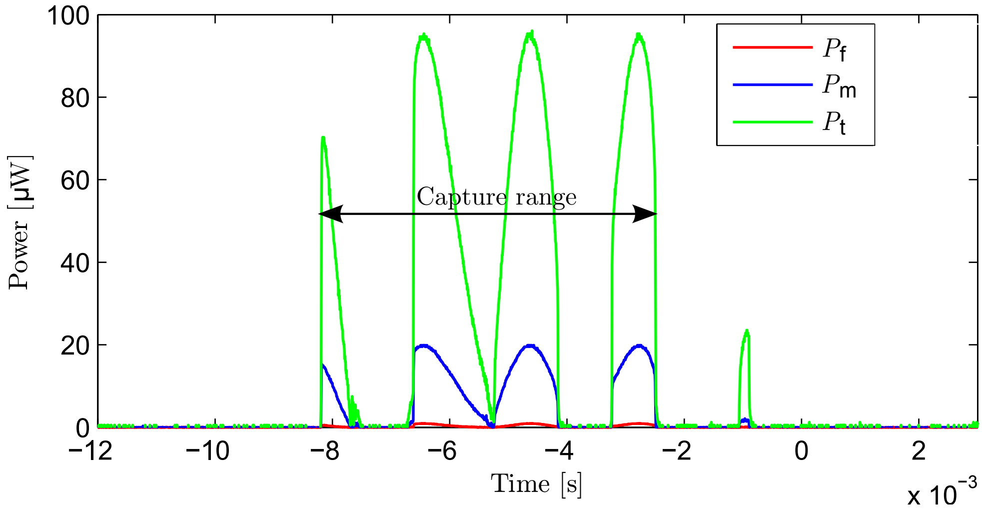

Figure 13: Data from a feedback measurement. We assume that the reason why we see several peaks instead of one broad is destructive interference in 'the long cavity' from feedback mirror to laser diode. The separation fits the FSR determined by the length of 'the long cavity'. It is assumed that the rightmost peak is a higher order mode, and it is therefore not included in the capture range.

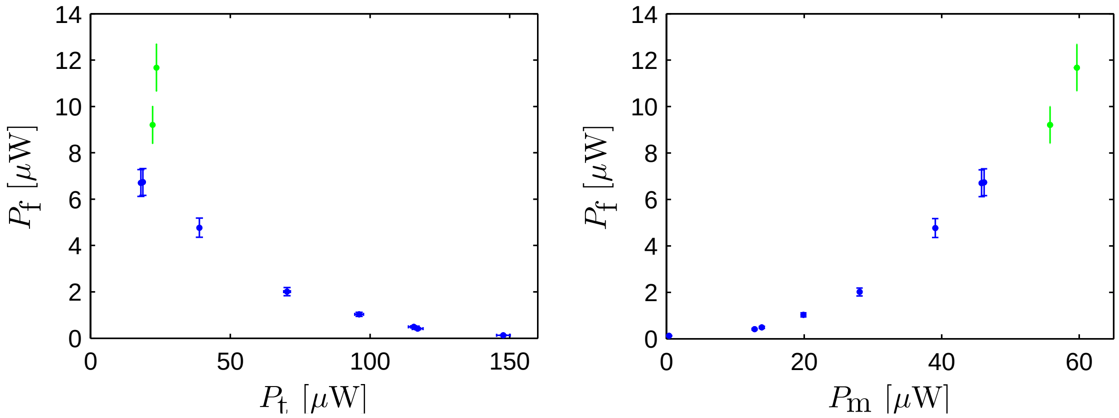

Figure 14: The left plot shows that the power fed back to the diode is not linearly proportional to transmitted power as expected. The right plot shows that this is not even the case for the power at the feedback mirror and the feedback power on the other side of the cavity. Either the coupling back into the Table Top Cavity is non-linear, or the photodiode measuring after the cavity is not linear for such small powers.
Green points are data from measurements where the polarizer was adjusted to putting more power through.

The power that reaches the diode will be less than the measured power, P_f, because of the losses in the optical elements (fiber, grating, laser diode facet etc.). Doing the measurement the fiber coupling was inefficient and an estimate of the fraction of the measured feedback power that is actually reaching the diode would be 10%. The laser output power is approximately 15 mW meaning that the feedback power ratio is $2\,\mu\mathrm{W}/(10 \cdot 15\,\mathrm{mW}) \approx 3 \cdot 10^{-5} \approx -50\,\mathrm{dB}$ for the optimal capture range. According to [Tkack & Chraplyvy] this is in a regime where the laser diode is subject to rapid mode jumping, but close to a regime of stability and narrow linewidth ($>-45\,\mathrm{dB}$). They use a distributed feedback laser diode, and the reason for the disagreement on optimal feedback power ratio could be due to differences of the diode types.

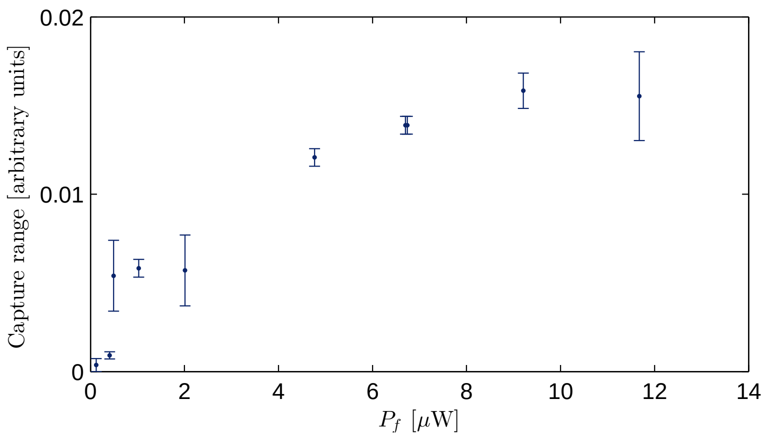

Figure 15: Capture range vs. feedback power. The capture range is measured from the Table Top Cavity sweep and is not calibrated to frequency, and the varying uncertainties come from difficulties determining which peaks are captured 00-mode and which are not. For instance for the data in Figure 13 the rightmost peak is not included. Despite this, the plot shows the connection between the feedback power and the capture range. The jumps in capture range are more peaks showing up for higher powers.

C Hänsch-Couillaud Lock

In 1980 T. W. Hänsch and B. Couillaud proposed a scheme for laser frequency stabilization, [Hänsch & Couillaud]. The central part in the scheme is generating an error signal that will clearly show when the laser is drifting away from the desired frequency. Their idea was to use an optical cavity to generate the signal. The following presents the scheme for the use in our setup with triangular cavities while the original proposal was to use a confocal cavity.

The scheme exploits the feature that the two linear polarizations are not resonant with the cavity for the same frequency (see section 2.1). The cavity is configured to be on resonance with the high-finesse polarization for the desired laser frequency (for locking we will always be using the Gaussian 00-mode since this is the desired mode), and, though it is resonant, some light will still be reflected, cf. (7) and (9). The low-finesse polarization light will be reflected almost completely, and this serves as a reference. Note that the incoming beam is linearly polarized because of the polarizer in front of the Table Top Cavity.

To detect the error signal we send the reflected beam through a quarter-wave plate and use a polarizing beam splitter (PBS) to split the signal onto the two photodiodes of a differential photo detector. The quarter-wave plate is rotated 45° with respect to the PBS axis which is parallel to the cavity plane.

For exact laser resonance the reflected high-finesse polarized (HF) light will not have acquired any phase shift, and the total reflected beam is still linearly polarized although the polarization is turned. If the laser is not resonant, the HF light will acquire a phase:

$$\phi = (k_\mathrm{l} - k_\mathrm{cav})L = \frac{2\pi\delta\nu L}{c}\,, \tag{40}$$

where $k_\mathrm{l}, k_\mathrm{cav}$ is the wave number for the laser beam and the cavity mode, respectively, and $\delta\nu = \nu_\mathrm{l} - \nu_\mathrm{cav}$ is the laser detuning. Using (4) and (5) we can express the reflected HF light:

$$\begin{aligned}
E_\mathrm{HF} &= E_\mathrm{HF}^\mathrm{in}\left(\sqrt{R_1} - \frac{T_1\sqrt{R_2R_3}e^{i\phi}}{1-\sqrt{R_1R_2R_3}e^{i\phi}}\right) \\
&= E_\mathrm{HF}^\mathrm{in}\left(\sqrt{R_1} - \frac{T_1}{\sqrt{R_1}}\frac{\sqrt{R_1R_2R_3}e^{i\phi}}{1-\sqrt{R_1R_2R_3}e^{i\phi}}\right) \\
&= E_\mathrm{HF}^\mathrm{in}\left(\sqrt{R_1} - \frac{T_1\sqrt{R_1R_2R_3}}{\sqrt{R_1}}\frac{\cos\phi - \sqrt{R_1R_2R_3} + i\sin\phi}{(1-\sqrt{R_1R_2R_3})^2 + 4\sqrt{R_1R_2R_3}\sin^2\frac{\phi}{2}}\right)\,,
\end{aligned} \tag{41}$$

where the sign alteration from (4) and (5) is made because we are in the p-polarization.

That means for an off-resonant laser beam there will be a phase mismatch of the HF light with reference to the LF light resulting in an elliptical polarization of the reflected beam. This is the error signal.

The quarter-wave plate introduces a $\pi/2$ phase delay s-polarized light, i.e. the transform $E_\mathrm{s} + E_\mathrm{p} \to iE_\mathrm{s} + E_\mathrm{p}$, with respect to the quarter-wave plate p and s axes. The transformation through the quarter-wave plate can then be written as:

$$\begin{pmatrix} E'_\mathrm{LF} \\ E'_\mathrm{HF} \end{pmatrix} = \begin{pmatrix} 1 & -1 \\ 1 & 1 \end{pmatrix}\begin{pmatrix} 1 & 0 \\ 0 & i \end{pmatrix}\begin{pmatrix} 1 & 1 \\ -1 & 1 \end{pmatrix}\begin{pmatrix} E_\mathrm{LF} \\ E_\mathrm{HF} \end{pmatrix}, \tag{42}$$

where the two outer matrices rotate into the quarter-wave plate frame and back. The differential detector will detect a signal $D \propto |E'_\mathrm{LF}|^2 - |E'_\mathrm{HF}|^2$. Using (42) this is:

$$\begin{aligned}
D &\propto |E_\mathrm{LF}e^{i\pi/4} + E_\mathrm{HF}e^{-i\pi/4}|^2 - |E_\mathrm{LF}e^{-i\pi/4} + E_\mathrm{HF}e^{i\pi/4}|^2 \\
&= 2i(E_\mathrm{LF}E^*_\mathrm{HF} - E^*_\mathrm{LF}E_\mathrm{HF}) = 4E_\mathrm{LF}\mathcal{I}[E^*_\mathrm{HF}] && (43) \\
&= -4E_\mathrm{LF}\frac{T_1\sqrt{R_1R_2R_3}}{\sqrt{R_1}}\frac{\sin\phi}{(1-\sqrt{R_1R_2R_3})^2 + 4\sqrt{R_1R_2R_3}\sin^2\frac{\phi}{2}}\,. && (44)
\end{aligned}$$

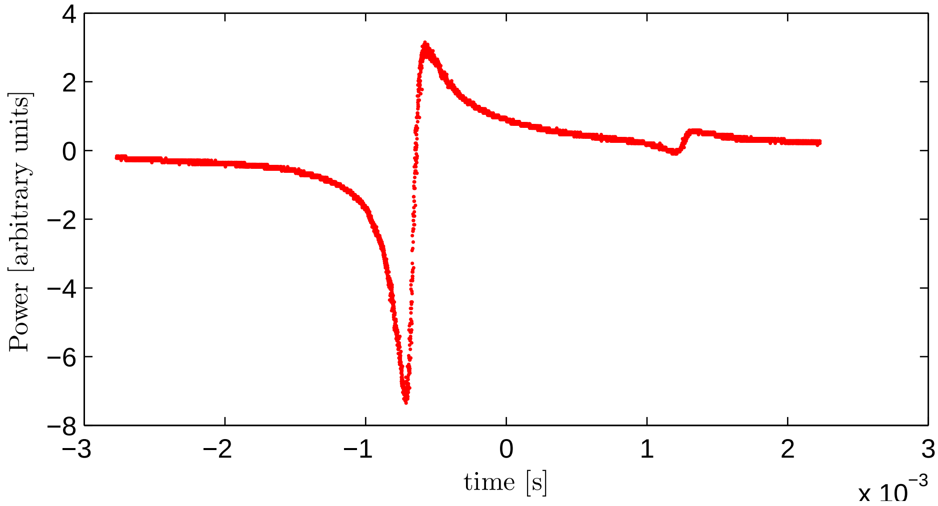

Figure 16: The Hänsch-Couillaud error signal from the Table Top Cavity. The steep curve makes it easy to lock to the cavity resonance where the error signal is zero. The little bump on the right side is the error signal for another weaker mode.

An example of the error signal D is shown in Figure 16.

The half-wave plate in front of the cavity (see Figure 6) can be turned to control the power of the error signal, E_{LF}. The signal is used to control the optical feedback from the feedback mirror on the transmission side of the cavity. To feed the light back the reflected light from the feedback mirror must interfere constructively with the laser light. The laser frequency is pulled to cavity resonance by controlling the feedback mirror position with the piezo behind it using the error signal through a PID controller. The range for which the laser frequency can be pulled depends on the feedback power (see Appendix B).

D Hermite-Gaussian Mode Profiles

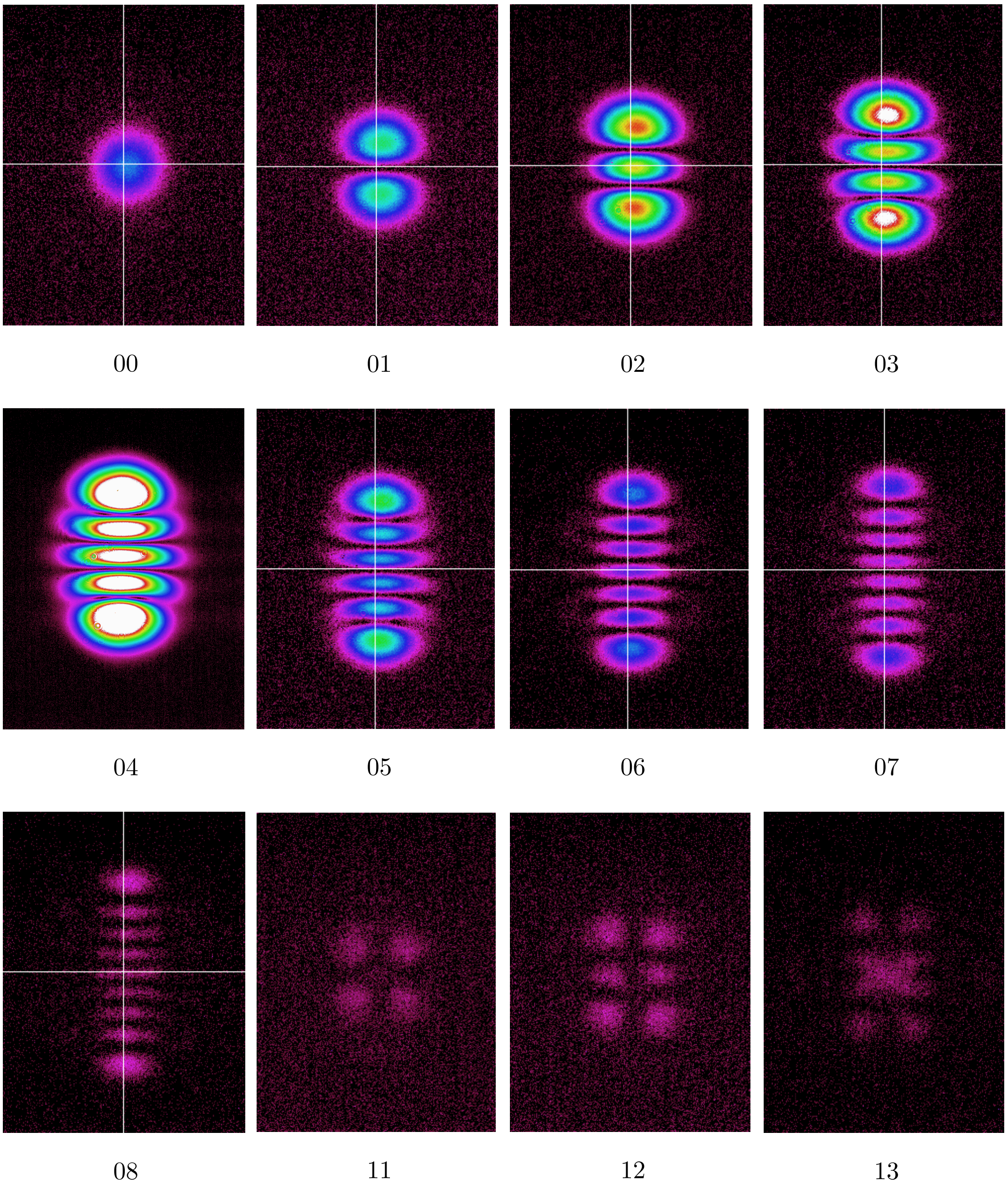

Figure 17: Pictures of the identified modes of The Evacuable Cavity taken with a camera behind the curved cavity mirror. The 13-mode is very close to the 00-mode and therefore has a spot in the centre.

E MATLAB-script

The used MATLAB-script consists of two scripts and three functions:

```
%Mode distribution
clear
set(0,'DefaultFigureWindowStyle','docked')
N=8; %How high I go in transversal modes

l=0;
m=0;

Ticks={};

for i=1:N+1
    for j=1:N+1
        [I, Inorm]=ModeOverlap3(l,m);
        str=['eta' num2str(l) num2str(m) '=matlabFunction(I);'];
        eval(str);
        str=['etanorm' num2str(l) num2str(m) '=matlabFunction(Inorm);'];
        eval(str);
        m=m+2;
    end
    l=l+2;
    m=0;
end

w2=6.891504e-04;%Calculated waist size of the cavity gaussian mode. Cavity 1.
w0=w2*0.66; %Trial waist size of incoming beam
z=-510e-3; %Trial waist position offset

k=2*pi/852.2e-9; %Wavenumber
z0=pi*w0^2/852.2e-9; %Rayleigh length
w1=w0*sqrt(1+z^2/z0^2); %Spot size at overlap
R=z+z0^2/z; %ROC

beta=1/w2^2+1/w1^2-1i*k/(2*R);

eta=[];
l=0;
m=0;

for i=1:N+1
    for j=1:N+1
        if l==0 && m==0
            str=['eta(' num2str(i) ',' num2str(j) ')=abs(eta' num2str(l) ...
            num2str(m) '(beta))^2;'];
        else
            str=['eta(' num2str(i) ',' num2str(j) ')=abs(eta' num2str(l) ...
            num2str(m) '(beta,w1))^2;'];
        end

        eval(str);
        str=['eta(' num2str(i) ',' num2str(j) ')=eta(' num2str(i) ',' num2str(j) ...
```

```
        ')/etanorm' num2str(l) num2str(m) '(w1);'];
        eval(str);

        m=m+2;
    end
    l=l+2;
    m=0;
end

%Further normalization
eta=eta./(pi/2*w2^2);

etavector=[];
%Plotting
for i=1:N+1
    for j=1:i
        etavector=[etavector eta(i,j)];
        Ticks(end+1)={[num2str((i-1)*2) num2str((j-1)*2)]};
    end
end
figure
bar(etavector)
set(gca,'XTick',1:sum(1:N+1),'XTickLabel',Ticks)
title(['Power distribution, $z''=' num2str(z) '$m, $w_b/w_{cav}=' num2str(w0/w2) ...
'$'],'interpreter','latex','FontSize',10)
set(gca,'YScale','log')
ylabel('$P_{lm}$','interpreter','latex','FontSize',10)
xlabel('$lm$-mode','interpreter','latex','FontSize',10)
```

```
function [I Inorm]=ModeOverlap3(l,m)

syms x y b w1
assume(real(b)>0)
assume(w1>0)

Hx=hermit(l,x);
Hy=hermit(m,y);

xint=Hx*exp(-b*x^2);
yint=Hy*exp(-b*y^2);

Ix=int(xint,x,-inf,inf);

Iy=int(yint,y,-inf,inf);

%Normalization
xnorm=Hx^2*exp(-2*x^2/w1^2);
ynorm=Hy^2*exp(-2*y^2/w1^2);
Inormx=int(xnorm,x,-inf,inf);
Inormy=int(ynorm,y,-inf,inf);
Inorm=Inormx*Inormy;

I=Iy*Ix;
```

```
end
```

```
function [sym]=hermit(n,var)

syms w1

[coef]=Hcoefficients(n);

sym=coef(1)*var^0;

for i=1:n
    sym=sym+coef(i+1)*(sqrt(2)*var/w1)^(i);
end
end
```

```
function [coef]=Hcoefficients(n)

if n==0
    coef=1;
elseif n==1
    coef=[0 2];
else

a=[1 0];
b=[0,2];

coef=[];
for i=2:n
    coef(1)=-2*(i-1)*a(1);
    for k=2:length(b)
        coef(k)=2*b(k-1)-2*(i-1)*a(k);
    end
    coef(end+1)=2*b(end);
    a=[b 0];
    b=coef;
end
end
```

```
%Ringcavity
%Calculates properties of the ring cavity filtering the single photon
close all;%clear;clc;
set(0,'DefaultFigureWindowStyle','docked')

nom=N; %Number of modes from ModeDistribution calculation

%Parameters
R1=0.9991;%Plane mirror reflectivity.
R3=0.99996;%Curved mirror reflectivity. Include losses here.
L1=1.495;%meters. Cavity roundtrip length
ROC1=5.23;%meters. Curved mirror radius of curvature
```

```
lambda=852.2e-9;%meters
loss=22;%Low-finesse loss factor

%wavenumber
k=2*pi/lambda;

%Singh finesse
Fsingh=4*R1*sqrt(R3)/(1-R1*sqrt(R3))^2;

%Singh finesse Low-finesse pol.
FsinghLF=4*(1-(1-R1)*loss)*sqrt(R3)/(1-(1-(1-R1)*loss)*sqrt(R3))^2;

ROC=ROC1;
L=L1

%Cavity transmission
Tmax=(1-R1)^2/(1-R1*sqrt(R3))^2;
TmaxLF=((1-R1)*loss)^2/(1-(1-(1-R1)*loss)*sqrt(R3))^2;
range=0.00005;%percent of k
x=linspace(k-k*range/100,k+k*range/100,100000);
Tp=Tmax./(1+Fsingh*sin(x*L/2).^2);%p-polarization
Ts=Tmax./(1+Fsingh*cos(x*L/2).^2);%s-pol.
fprintf('Tmax: %d\n',Tmax)

%Finesse
F=pi/2*sqrt(Fsingh);
fprintf('Finesse: %d\n',F)

%HF Linewidth (wavenumber)
dk=2/sqrt(Fsingh)/L;
fprintf('Linewidth: %d (wavenumber)\n',dk)
dv=dk*299792458/2/pi;
fprintf('HF Linewidth HWHM: %d (freq.) from round trip calculation\n',dv)

%LF linewidth
dk=2/sqrt(FsinghLF)/L;
dv=dk*299792458/2/pi;
fprintf('LF Linewidth HWHM: %d (freq.) from round trip calculation\n',dv)

%Waist size
w0=sqrt(lambda/(2*n*pi))*(L*(2*ROC-L))^(1/4);
fprintf('Waist size: %d m\n',w0)

%Rayleigh length
z0=pi*w0^2/lambda;
fprintf('Rayleigh length: %d m\n',z0)

%Free Spectral Range
FSR=299792458/L;
fprintf('FSR: %d Hz\n',FSR)

%Photon lifetime linewidth broadening (frequency)
Loss=3-2*R1-R3;
Tc=n*L/299792458/Loss;
```

```
dv=1/2/pi/Tc;%FWHM
fprintf('Linewidth: %d (freq.) from cavity lifetime\n\n',dv)

%Frequency shift for transversal modes
a=acos(1-L/ROC)/pi/2*299792458/L;
fprintf('Alpha: %d Hz\n',a)

%Difference on FSR scale for 9.2 GHz
filt=-9192631770+FSR*46;
fprintf('Filter freq. difference: %d Hz\n\n',filt)

%Drawing the resonances
figure
xlabel('$\Delta\nu$ [Hz]','interpreter','latex')
set(gca,'YTick',[],'FontSize',8)
hold on
xlim([0 FSR])
str=sprintf('Cavity %d FSR spectrum',i);
title(str,'interpreter','latex','FontSize',10)

line([0 0],[0 1],'LineWidth',1)
line([FSR FSR],[0 1],'LineWidth',1)
for j=1:no %higher order modes for both pol.s
    line([a*j a*j],[0 1/(1+j)],'LineWidth',1)
    line([a a]*j+FSR/2,[0 1/(1+j)],'LineWidth',1,'Color',[0 1 0])
    line([a a]*j+FSR/2-FSR,[0 1/(1+j)],'LineWidth',1,'Color',[0 1 0])
end
line([a a]*8-FSR,[0 1/9],'LineWidth',1)
line([1 1]*FSR/2,[0 1],'LineWidth',1,'LineStyle','-.','Color',[0 0 0])

%LF polarization including offset
for j=1:9
    line([1 1]*(-0.529+j-1)*a+FSR/2,[0 1/(1+j)],'Color',[0 0 0],'LineWidth',1)
    line([1 1]*(-0.529+j-1)*a-FSR/2,[0 1/(1+j)],'Color',[0 0 0],'LineWidth',1)
end

line([filt filt],[0 1],'Color',[1 0 0],'LineWidth',1) %filter freq.

%Filter ratio
PhiFilt=filt/FSR*2*pi;

xsiLF=[];
xsiHF=[];

for q=1:nom+1
    l=(q-1)*2;
    for j=1:nom+1
        m=(j-1)*2;
        %HF polarization
        g=Tmax/(1+Fsingh*sin((PhiFilt-(l+m)*acos(1-L/ROC)+pi/2*(1-(-1)^m))/2).^2);
        %fprintf([num2str(l) num2str(m) ' p-pol Filter ratio: %d\n'],g)
        xsiHF=[xsiHF g*eta(q,j)];

        %LF polarization
```

```
        g=TmaxLF/(1+FsinghLF*cos((PhiFilt-(l+m-0.529)*acos(1-L/ROC)+ ...
        pi/2*(1-(-1)^m))/2).^2);
        %fprintf([num2str(l) num2str(m) ' s-pol Filter ratio: %d\n'],g)
        xsiLF=[xsiLF g*eta(q,j)];
    end
end
fprintf('\nCavity resonant with single photon HF:\nTotal LF Filter ratio: ...
%d\n',sum(xsiLF))
fprintf('Total HF Filter ratio: %d\n',sum(xsiHF))

xsiLF=[];
xsiHF=[];
for q=1:nom+1
    l=(q-1)*2;
    for j=1:nom+1
        m=(j-1)*2;
        %LF polarization
        g=TmaxLF/(1+FsinghLF*sin((PhiFilt-(l+m)*acos(1-L/ROC)+ ...
        pi/2*(1-(-1)^m))/2).^2);
        %fprintf([num2str(l) num2str(m) ' p-pol Filter ratio: %d\n'],g)
        xsiLF=[xsiLF g*eta(q,j)];

        %HF polarization
        g=Tmax/(1+Fsingh*cos((PhiFilt-(l+m+0.529)*acos(1-L/ROC)+ ...
        pi/2*(1-(-1)^m))/2).^2);
        %fprintf([num2str(l) num2str(m) ' s-pol Filter ratio: %d\n'],g)
        xsiHF=[xsiHF g*eta(q,j)];
    end
end
fprintf('\nCavity resonant with single photon LF:\nTotal LF Filter ratio: ...
%d\n',sum(xsiLF))
fprintf('Total HF Filter ratio: %d\n',sum(xsiHF))
```